Physics of Plasmas

RESEARCH ARTICLE | APRIL 18 2024

Nonlinear coupling of tearing modes in reversed field pinch plasmas with stepped pressure profiles

R. Fitzpatrick

Check for updates

Phys. Plasmas 31, 042510 (2024)
https://doi.org/10.1063/5.0203908

View Online
Export Citation

23 April 2024 14:39:08

AIP Advances
Why Publish With Us?
25 DAYS average time to 1st decision
740+ DOWNLOADS average per article
INCLUSIVE scope
Learn More
AIP Publishing

AIP Publishing

Nonlinear coupling of tearing modes in reversed field pinch plasmas with stepped pressure profiles

Cite as: Phys. Plasmas **31**, 042510 (2024); doi: 10.1063/5.0203908
Submitted: 17 February 2024 · Accepted: 2 April 2024 ·
Published Online: 18 April 2024

View Online Export Citation CrossMark

R. Fitzpatrick[a)]

AFFILIATIONS

Institute for Fusion Studies, Department of Physics, University of Texas at Austin, Austin, Texas 78712, USA

[a)]Author to whom correspondence should be addressed: rfitzp@utexas.edu

ABSTRACT

A theory of the three-wave coupling of triplets of tearing modes in toroidal pinches [i.e., either reversed field pinches (RFPs) or tokamaks] was proposed by R. Fitzpatrick [Phys. Plasmas **6**, 1168 (1999)]. However, this theory only applies to toroidal pinches with negligible equilibrium plasma pressure gradients. Such a limitation is particularly inappropriate to RFPs. This paper generalizes the analysis of R. Fitzpatrick [Phys. Plasmas **6**, 1168 (1999)] in order to take the equilibrium pressure gradient into account. However, for the sake of simplicity, a stepped pressure profile, rather than a continuous profile, is employed. In the limit in which the number of steps becomes very large, the results obtained from the generalized theory are presumably equivalent to those that would have been achieved using a continuous pressure profile. The generalized theory is used to investigate the formation of the characteristic toroidally localized pattern of phase-locked $m = 1$ and $m = 0$ tearing modes in RFP plasmas that is known as the "slinky" pattern. The incorporation of the equilibrium plasma pressure into the analysis is found to be of crucial importance when determining the properties of the pattern. This is the case because the plasma pressure controls the number of unstable $m = 1$ and $m = 0$ tearing modes, and also significantly affects the strength of three-wave coupling, as well as the phase relation between the phase-locked $m = 1$ and $m = 0$ modes.

© 2024 Author(s). All article content, except where otherwise noted, is licensed under a Creative Commons Attribution (CC BY) license (https://creativecommons.org/licenses/by/4.0/). https://doi.org/10.1063/5.0203908

23 April 2024 14:39:08

I. INTRODUCTION

This paper investigates the nonlinear coupling of tearing modes in reversed field pinches (RFPs). At its most basic level, such coupling involves a triplet of modes that satisfy the three-wave coupling relation $(m_1, n_1) + (m_2, n_2) = (m_3, n_3)$, where m denotes a poloidal mode number and n a toroidal mode number. Moreover, the strength of the coupling characteristically scales as the *square* of the mode amplitude, whereas the electromagnetic torques that develop in the plasma as a consequence of the coupling scale as the *cube* of the mode amplitude. Like a tokamak,[1] a RFP is an axisymmetric toroidal device that confines a plasma on a set of nested toroidal magnetic flux-surfaces.[2,3] However, RFPs have weaker toroidal magnetic fields, relative to the poloidal field, than tokamaks and are consequently much more unstable to macroscopic magnetohydrodynamical (MHD) instabilities such as tearing modes.[4–6] Indeed, the saturated amplitude of tearing modes (relative to the amplitude of the equilibrium magnetic field) is typically, at least, an order of magnitude greater in RFPs than in tokamaks. Consequently, the nonlinear coupling of tearing modes is much more prevalent in RFPs than in tokamaks. For example, the characteristic relaxation cycle of RFP plasmas, which periodically broadens the parallel current profile, and thereby maintains the reversal of the toroidal magnetic field, is associated with the nonlinear coupling of $m = 1$ tearing modes, resonant in the plasma core, to $m = 0$ tearing modes, resonant at the reversal surface (where the equilibrium toroidal magnetic field changes direction).[7–10] The same coupling leads to the formation of the commonly observed, toroidally localized, phase-locked pattern of multiple $m = 1$ and $m = 0$ tearing modes that is known as the *slinky* pattern.[11–13] Note, however, that the nonlinear coupling of tearing modes has also been observed in tokamak plasmas.[14–16] In particular, nonlinear coupling is inferred to play a role in the triggering of neoclassical tearing modes in tokamaks,[17] which is often associated with the interaction of two modes that do not couple directly, such as the (1, 1) and the (4, 3), but could conceivably couple via an intermediate mode; in this example, the (3, 2). Indeed, a clear observation of this exact process is described in Ref. 16.

A theory of the three-wave coupling of triplets of tearing modes in toroidal pinches (i.e., either RFPs or tokamaks) was proposed in Ref. 18. This theory was subsequently employed to investigate the formation of the slinky pattern in RFPs,[19] and the coupling of neoclassical tearing modes in tokamaks.[20] However, the theory has a serious

© Author(s) 2024

limitation. Namely, it only applies to toroidal pinches with *negligible* equilibrium plasma pressure gradients. Such a limitation is particularly inappropriate to RFPs. The aim of this paper is to remove the limitation, and, thus, to develop a theory of the three-wave coupling of tearing modes in finite-pressure toroidal pinches. Unfortunately, a direct generalization of the analysis of Ref. 18 using a continuous equilibrium pressure profile is prohibitively difficult. [This can be appreciated from an examination of Eq. (56), which illustrates how the inclusion of equilibrium pressure gradients leads to a very large number of additional terms in the linear eigenmode equation of a given tearing mode.] However, inspired by recent research,[21,22] we have discovered that the analysis of Ref. 18 can be generalized in a relatively straightforward manner on the assumption that the equilibrium plasma pressure profile is *stepped*. Indeed, as described in this paper, in the limit in which the number of steps becomes very large, results can be achieved that are presumably equivalent to those that would have been achieved had we found a way of directly incorporating a continuous pressure profile into the analysis.

Alternative or complementary theories to that proposed in Ref. 18 were proposed in Refs. 23–26. The theory proposed in Ref. 23 predicts the same structure of three-wave coupling between tearing mode triplets as that proposed in Ref. 18, but employs assumptions that are only valid in tokamaks, and also neglects equilibrium plasma pressure gradients. The theory presented in Ref. 24 is based on that of Ref. 23, only applies to tokamaks, and neglects equilibrium plasma pressure gradients. The theory presented in Ref. 25 seems to imply that three-wave coupling in RFPs depends crucially on the variation of the magnetic field-strength around magnetic flux-surfaces due to toroidicity. However, as demonstrated in Ref. 18, to lowest order, three-wave coupling in RFPs is a cylindrical effect. Finally, the theory presented in Ref. 26 is based on that in Ref. 18, but neglects equilibrium plasma pressure gradients.

This paper is organized as follows. After some preliminary analyses in Sec. II, we introduce the idea of a stepped pressure equilibrium in Sec. III. In Sec. IV, we give a more complete and self-consistent version of the nonlinear mode coupling theory developed in Ref. 18. Likewise, in Sec. V, we give a more complete and self-consistent version of the theory of slinky pattern formation in RFPs that was presented in Ref. 19. Section VI discusses an example calculation that highlights the important role that equilibrium plasma pressure plays in the nonlinear coupling of tearing modes, and especially in the formation of the slinky pattern, in RFP plasmas. Finally, the paper is summarized in Sec. VII.

II. PRELIMINARY ANALYSIS

A. Plasma equilibrium

Consider a thermonuclear plasma confined in a conventional toroidal pinch.[4] For the case of an RFP, the equilibrium is very well approximated as a periodic cylinder of circular cross section. Let r, θ, z be right-handed cylindrical coordinates, and let $\mathbf{e}_r = \nabla r/|\nabla r|$, $\mathbf{e}_\theta = \nabla\theta/|\nabla\theta|$, and $\mathbf{e}_z = \nabla z/|\nabla z|$ be the corresponding unit vectors. The system is assumed to be periodic in the z-direction with periodicity length $2\pi R_0$, where R_0 is the simulated major radius of the plasma. It is convenient to define the simulated toroidal angle $\phi = z/R_0$, as well as the corresponding simulated unit vector $\mathbf{e}_\phi = \nabla\phi/|\nabla\phi| = \mathbf{e}_z$. Finally, let a be the minor radius of the plasma.

The equilibrium magnetic field is written

$$\mathbf{B} = B_\theta(r)\,\mathbf{e}_\theta + B_\phi(r)\,\mathbf{e}_\phi. \tag{1}$$

The equilibrium plasma current density takes the form

$$\mu_0\,\mathbf{J} = \nabla\times\mathbf{B} = -B_\phi'\,\mathbf{e}_\theta + \frac{(r\,B_\theta)'}{r}\,\mathbf{e}_\phi, \tag{2}$$

where $'$ denotes d/dr. Note that

$$\nabla\cdot\mathbf{B} = \nabla\cdot\mathbf{J} = 0, \tag{3}$$

in accordance with Maxwell's equations and charge conservation, and

$$(\mathbf{J}\cdot\nabla)\,\mathbf{B} - (\mathbf{B}\cdot\nabla)\,\mathbf{J} = \mathbf{0}. \tag{4}$$

The safety-factor profile is written[4]

$$q(r) = \frac{\epsilon\,B_\phi}{B_\theta}, \tag{5}$$

where

$$\epsilon(r) = \frac{r}{R_0} \tag{6}$$

is the inverse aspect-ratio profile.

Equilibrium force balance requires that[4]

$$\mathbf{J}\times\mathbf{B} = \nabla P, \tag{7}$$

where $P(r)$ is the equilibrium pressure profile. It follows from Eq. (2) that

$$B_\phi' = -\frac{\sigma}{a}\,B_\theta - \frac{\mu_0\,P'\,B_\phi}{B^2}, \tag{8}$$

$$B_\theta' + \frac{B_\theta}{r} = \frac{\sigma}{a}\,B_\phi - \frac{\mu_0\,P'\,B_\theta}{B^2}, \tag{9}$$

where $\sigma(r)$ is a dimensionless function that specifies the equilibrium parallel current density. Of course, $P = \sigma = 0$ in the vacuum region, $r > a$, surrounding the plasma. The previous two equations can be combined to give the force balance constraint,[4]

$$0 = \left(\mu_0\,P + \frac{B_\theta^2 + B_\phi^2}{2}\right)' + \frac{B_\theta^2}{r}, \tag{10}$$

as well as

$$r\,q' = 2\,q - \frac{\sigma}{\epsilon_a}\,(\epsilon^2 + q^2), \tag{11}$$

where $\epsilon_a = a/R_0$. The previous equation implies that the safety-factor profile in a (cylindrical) toroidal pinch is determined solely by the parallel current profile and is completely independent of the pressure profile.

B. Perturbed plasma equilibrium

Let us assume that the plasma equilibrium is stable to rapidly growing (i.e., growing on timescales comparable to the Alfvén time) ideal-MHD modes, but is perturbed by multiple slowly growing (i.e., growing on timescales that are much longer than the Alfvén time) tearing modes.[6] It follows that the perturbed plasma equilibrium is governed by the perturbed force balance equation[4,6]

23 April 2024 14:39:08

© Author(s) 2024

$$(\mathbf{J}+\mathbf{j})\times(\mathbf{B}+\mathbf{b}) = \nabla(P+p). \tag{12}$$

Here, **b**, **j**, and p are the perturbed magnetic field, plasma current density, and pressure, respectively. The neglect of plasma inertia in the previous equation is justified because tearing modes evolve on timescales that are much longer than the Alfvén time.[6] Furthermore, nonideal terms, such as plasma resistivity and viscosity, are much smaller in magnitude than the leading order terms, and can, therefore, safely be neglected in the previous equation.[4,6] Note that plasma inertia, resistivity, and viscosity must be taken into account in a number of radially thin regions of the plasma in which ideal force balance breaks down[6,27] (see Sec. III B). We shall asymptotically match our ideal solutions across these regions.[6,28,29]

Maxwell's equations (neglecting the displacement current, because we are dealing with slowly growing perturbations) imply that

$$\nabla\cdot\mathbf{b} = 0, \tag{13}$$

$$\mu_0\,\mathbf{j} = \nabla\times\mathbf{b}. \tag{14}$$

It follows from the previous equation that

$$\nabla\cdot\mathbf{j} = 0. \tag{15}$$

The curl of μ_0 times Eq. (12) yields

$$(\mu_0\,\mathbf{j}\cdot\nabla)\,\mathbf{B} + (\mu_0\,\mathbf{J}\cdot\nabla)\,\mathbf{b} - (\mathbf{b}\cdot\nabla)\,(\mu_0\,\mathbf{J}) - (\mathbf{B}\cdot\nabla)\,(\mu_0\,\mathbf{j}) = \mathbf{A}, \tag{16}$$

where

$$\mathbf{A} \equiv \nabla\times(\mu_0\,\mathbf{j}\times\mathbf{b}) = (\mathbf{b}\cdot\nabla)\,(\mu_0\,\mathbf{j}) - (\mu_0\,\mathbf{j}\cdot\nabla)\,\mathbf{b}, \tag{17}$$

and use has been made of Eqs. (3), (4), (13), and (15). The previous equation implies that

$$\nabla\cdot\mathbf{A} = 0. \tag{18}$$

(Note, incidentally, that **A** does *not* denote the magnetic vector potential in this paper.)

C. Perturbed quantities

A general perturbed vector quantity associated with multiple tearing modes can be written in the form

$$\mathbf{a}(\mathbf{r},t) = \sum_{m,n}\mathbf{a}^{m,n}(r,t)\,\mathrm{e}^{\mathrm{i}(m\theta-n\phi)}, \tag{19}$$

where

$$\mathbf{a}^{m,n}(r,t) = a_r^{m,n}(r,t)\,\mathbf{e}_r + a_\theta^{m,n}(r,t)\,\mathbf{e}_\theta + a_\phi^{m,n}(r,t)\,\mathbf{e}_\phi. \tag{20}$$

Here, m and n are poloidal and toroidal mode numbers, respectively.

Let

$$F^{m,n}(r) = m\,B_\theta - n\,\epsilon\,B_\phi, \tag{21}$$

$$G^{m,n}(r) = n\,\epsilon\,B_\theta + m\,B_\phi, \tag{22}$$

$$H^{m,n}(r) = m^2 + (n\,\epsilon)^2. \tag{23}$$

The radial component of the (m, n) harmonic of Eq. (16) yields

$$\mu_0\,j_r^{mn} = -\frac{(G^{m,n})'}{F^{m,n}}\,b_r^{m,n} + \frac{r}{F^{m,n}}\,\mathrm{i}A_r^{m,n}, \tag{24}$$

where use has been made of Eq. (2). Likewise, the θ-component of the (m, n) harmonic of Eq. (16) gives

$$\mu_0\,j_\theta^{m,n} = -\frac{(G^{m,n})'}{F^{m,n}}\,b_\theta^{m,n} + \left[\left(\frac{B_\theta}{r}\right)'\frac{(G^{m,n})'}{F^{m,n}} - \left(\frac{B_\phi'}{r}\right)'\right]\frac{r^2}{F^{m,n}}\,\mathrm{i}b_r^{m,n} + \left(\frac{B_\theta}{r}\right)'\frac{r^3}{(F^{m,n})^2}\,A_r^{m,n} + \frac{r}{F^{m,n}}\,\mathrm{i}A_\theta^{m,n}. \tag{25}$$

Finally, the ϕ-component of the (m, n) harmonic of Eq. (16) yields

$$\mu_0\,j_\phi^{m,n} = -\frac{(G^{m,n})'}{F^{m,n}}\,b_\phi^{m,n} + \left[B_\phi'\,\frac{(G^{m,n})'}{F^{m,n}} + \left(\frac{[r\,B_\theta]'}{r}\right)'\right]\frac{r}{F^{m,n}}\,\mathrm{i}b_r^{m,n} + B_\phi'\,\frac{r^2}{(F^{m,n})^2}\,A_r^{m,n} + \frac{r}{F^{m,n}}\,\mathrm{i}A_\phi^{m,n}. \tag{26}$$

It is easily verified that

$$\frac{\partial(r\,j_r^{m,n})}{\partial r} + \mathrm{i}\,(m\,j_\theta^{m,n} - n\,\epsilon\,j_\phi^{m,n}) = 0, \tag{27}$$

as is required by Eq. (15), provided that

$$\frac{\partial(r\,A_r^{m,n})}{\partial r} + \mathrm{i}\,(m\,A_\theta^{m,n} - n\,\epsilon\,A_\phi^{m,n}) = 0, \tag{28}$$

as is required by Eq. (18).

The (m, n) harmonic of Eq. (13) and the radial component of the (m, n) harmonic of Eq. (14) yield

$$\frac{\partial(r\,b_r^{m,n})}{\partial r} = -\mathrm{i}\,(m\,b_\theta^{m,n} - n\,\epsilon\,b_\phi^{m,n}), \tag{29}$$

$$\mu_0\,r\,j_r^{m,n} = \mathrm{i}\,(n\,\epsilon\,b_\theta^{m,n} + m\,b_\phi^{m,n}), \tag{30}$$

respectively. The previous two equations can be inverted to give

$$b_r^{m,n}(r,t) = \frac{\mathrm{i}\,\psi^{m,n}(r,t)}{r}, \tag{31}$$

$$b_\theta^{m,n}(r,t) = -\frac{m}{H^{m,n}}\frac{\partial\psi^{m,n}}{\partial r} - \frac{n\,\epsilon}{H^{m,n}}\frac{(G^{m,n})'}{F^{m,n}}\,\psi^{m,n} + \frac{n\,\epsilon}{H^{m,n}}\frac{r^2}{F^{m,n}}\,A_r^{m,n}, \tag{32}$$

$$b_\phi^{m,n}(r,t) = \frac{n\,\epsilon}{H^{m,n}}\frac{\partial\psi^{m,n}}{\partial r} - \frac{m}{H^{m,n}}\frac{(G^{m,n})'}{F^{m,n}}\,\psi^{m,n} + \frac{m}{H^{m,n}}\frac{r^2}{F^{m,n}}\,A_r^{m,n}, \tag{33}$$

where use has been made of Eq. (24). Finally, Eqs. (24)–(26) yield

$$\mu_0\,j_r^{m,n}(r,t) = -\frac{(G^{m,n})'}{r\,F^{m,n}}\,\mathrm{i}\psi^{m,n} + \frac{r}{F^{m,n}}\,\mathrm{i}A_r^{m,n}, \tag{34}$$

$$\mu_0\,j_\theta^{m,n}(r,t) = \frac{m}{H^{m,n}}\frac{(G^{m,n})'}{F^{m,n}}\frac{\partial\psi^{m,n}}{\partial r} + \left[\frac{n\,\epsilon}{H^{m,n}}\frac{([G^{m,n}]')^2}{F^{m,n}} - r\left(\frac{B_\theta}{r}\right)'\frac{(G_{m,n})'}{F^{m,n}} + r\left(\frac{B_\phi'}{r}\right)'\right]\frac{\psi^{m,n}}{F^{m,n}} + \left[r\left(\frac{B_\theta}{r}\right)' - \frac{n\,\epsilon}{H^{m,n}}(G^{m,n})'\right]\frac{r^2}{(F^{m,n})^2}A_r^{m,n} + \frac{r}{F^{m,n}}\mathrm{i}A_\theta^{m,n}, \tag{35}$$

23 April 2024 14:39:08

© Author(s) 2024

$$\mu_0 j_\phi^{m,n}(r,t) = -\frac{n\,\epsilon}{H^{m,n}}\frac{(G^{m,n})'}{F^{m,n}}\frac{\partial\psi^{m,n}}{\partial r} + \left[\frac{m}{H^{m,n}}\frac{([G^{m,n}]')^2}{F^{m,n}} - B_\phi'\frac{(G_{m,n})'}{F^{m,n}} - \left(\frac{[r\,B_\theta]'}{r}\right)'\right]\frac{\psi^{m,n}}{F^{m,n}} + \left[B_\phi' - \frac{m}{H^{m,n}}(G^{m,n})'\right]\frac{r^2}{(F^{m,n})^2}A_r^{m,n} + \frac{r}{F^{m,n}}\mathrm{i}A_\phi^{m,n}. \tag{36}$$

The θ- and the ϕ-components of the (m, n) harmonics of Eq. (14) take the respective forms

$$\mu_0\, r\, j_\theta^{m,n} = -\mathrm{i}\,n\,\epsilon\, b_r^{m,n} - r\frac{\partial b_\phi^{m,n}}{\partial r}, \tag{37}$$

$$\mu_0\, r\, j_\phi^{m,n} = -\mathrm{i}\,m\, b_r^{m,n} + \frac{\partial(r\, b_\theta^{m,n})}{\partial r}. \tag{38}$$

Equations (31)–(38) give

$$0 = n\,\epsilon\,(u_r^{m,n} + U_r^{m,n}) - u_\theta^{m,n}\,\psi^{m,n} - U_\theta^{m,n}, \tag{39}$$

$$0 = m\,(u_r^{m,n} + U_r^{m,n}) - u_\phi^{m,n}\,\psi^{m,n} - U_\phi^{m,n}. \tag{40}$$

Here,

$$u_r^{m,n}(r,t) = \frac{\partial}{\partial r}\left[\frac{r}{H^{m,n}}\frac{\partial\psi^{m,n}}{\partial r}\right] - \frac{\psi^{m,n}}{r} + \frac{r}{H^{m,n}}\left[\frac{(G^{m,n})'}{F^{m,n}}\right]^2\psi^{m,n}, \tag{41}$$

$$u_\theta^{m,n}(r) = r\left[\frac{m}{H^{m,n}}\frac{(G^{m,n})'}{F^{m,n}}\right]' + r^2\left(\frac{B_\theta}{r}\right)'\frac{(G^{m,n})'}{(F^{m,n})^2} - r\left(\frac{B_\phi'}{r}\right)'\frac{r}{F^{m,n}}, \tag{42}$$

$$u_\phi^{m,n}(r) = -\left[\frac{n\,\epsilon}{H^{m,n}}\frac{r\,(G^{m,n})'}{F^{m,n}}\right]' + r\,B_\phi'\frac{(G^{m,n})'}{(F^{m,n})^2} + \left[\frac{(r\,B_\theta)'}{r}\right]'\frac{r}{F^{m,n}}, \tag{43}$$

$$U_r^{m,n}(r,t) = -\frac{r^3}{H^{m,n}}\frac{(G^{m,n})'}{(F^{m,n})^2}A_r^{m,n}, \tag{44}$$

$$U_\theta^{m,n}(r,t) = -r\frac{\partial}{\partial r}\left(\frac{m}{H^{m,n}}\frac{r^2}{F^{m,n}}A_r^{m,n}\right) - r\left(\frac{B_\theta}{r}\right)'\frac{r^3}{(F^{m,n})^2}A_r^{m,n} - \frac{r^2}{F^{m,n}}\mathrm{i}A_\theta^{m,n}, \tag{45}$$

$$U_\phi^{m,n}(r,t) = \frac{\partial}{\partial r}\left(\frac{n\,\epsilon}{H^{m,n}}\frac{r^3}{F^{m,n}}A_r^{m,n}\right) - B_\phi'\frac{r^3}{(F^{m,n})^2}A_r^{m,n} - \frac{r^2}{F^{m,n}}\mathrm{i}A_\phi^{m,n}. \tag{46}$$

Equations (39) and (40) require that

$$m\,(u_\theta^{m,n} + U_\theta^{m,n}) = n\,\epsilon\,(u_\phi^{m,n} + U_\phi^{m,n}), \tag{47}$$

for self-consistency. In fact, it is easily demonstrated that

$$m\,u_\theta^{m,n} = n\,\epsilon\,u_\phi^{m,n}, \tag{48}$$

and that

$$m\,U_\theta^{m,n} = n\,\epsilon\,U_\phi^{m,n}, \tag{49}$$

provided that Eq. (28) is satisfied.

Finally, Eqs. (39) and (40) yield

$$0 = H^{m,n}\,(u_r^{m,n} + U_r^{m,n}) - (n\,\epsilon\,u_\theta^{m,n} + m\,u_\phi^{m,n}) - (n\,\epsilon\,U_\theta^{m,n} + m\,U_\phi^{m,n}), \tag{50}$$

which reduces to the *nonlinear eigenmode equation*

$$\frac{\partial}{\partial r}\left(f^{m,n}\frac{\partial\psi^{m,n}}{\partial r}\right) - g^{m,n}\,\psi^{m,n} - V^{m,n} = 0, \tag{51}$$

where

$$f^{m,n}(r) = \frac{r}{H^{m,n}}, \tag{52}$$

$$g^{m,n}(r) = \frac{1}{r} + \frac{r^3}{H^{m,n}\,F^{m,n}}\left[\frac{1}{r}\left(\frac{F^{m,n}}{r}\right)'\right]' - \frac{2\,m\,n\,\epsilon\,(G^{m,n})'}{(H^{m,n})^2\,F^{m,n}} - \frac{2\,n\,\epsilon\,(G^{m,n})'\,B_\theta}{H^{m,n}\,(F^{m,n})^2} + \frac{4\,m\,r}{H^{m,n}\,F^{m,n}}\left(\frac{B_\theta}{r}\right)', \tag{53}$$

$$V_{m,n}(r,t) = \frac{2\,m\,n\,\epsilon}{(H^{m,n})^2\,F^{m,n}}\,r^2\,A_r^{m,n} + \frac{2\,n\,\epsilon\,B_\theta}{H^{m,n}\,(F^{m,n})^2}\,r^2\,A_r^{m,n} - \mathrm{i}\frac{r^2}{H^{m,n}\,F^{m,n}}\,(n\,\epsilon\,A_\theta^{m,n} + m\,A_\phi^{m,n}). \tag{54}$$

D. Linear eigenmode equation

If we neglect the nonlinear term (i.e., the term involving $V^{m,n}$) in the general eigenmode equation, (51), then it reduces to the following *linear eigenmode equation*:

$$\frac{\partial}{\partial r}\left(f^{m,n}\frac{\partial\psi_L^{m,n}}{\partial r}\right) - g^{m,n}\,\psi_L^{m,n} = 0. \tag{55}$$

Here, $\psi_L^{m,n}(r,t)$ is the linear eigenmode of a tearing perturbation possessing m periods in θ, and n periods in ϕ.

Making use of Eqs. (6), (8), (9), and (21)–(23), the expression for $g^{m,n}(r)$ given in Eq. (53) reduces to

$$g^{m,n}(r) = \frac{1}{r} + \frac{2\,m\,n\,\epsilon}{(H^{m,n})^2}\frac{\sigma}{a} - \frac{1}{H^{m,n}}\left[r\left(\frac{\sigma}{a}\right)^2 - \frac{\mu_0\,P'}{B^2} + \frac{r\,\mu_0\,P''}{B^2} + \frac{r\,(\mu_0\,P')^2}{B^4} + \frac{2\,B_\theta^2\,\mu_0\,P'}{B^4}\right] + \frac{G^{m,n}}{H^{m,n}\,F^{m,n}}\left(r\frac{\sigma'}{a} - 2\,r\frac{\sigma}{a}\frac{\mu_0\,P'}{B^2} + \frac{2\,m\,n\,\epsilon}{H^{m,n}}\frac{\mu_0\,P'}{B^2} + \frac{2\,n\,\epsilon\,B_\theta}{F^{m,n}}\frac{\mu_0\,P'}{B^2}\right). \tag{56}$$

Note that the final term on the right-hand side of the previous equation ensures that $\psi_L(x) \propto |x|^{\nu_L}$, $|x|^{\nu_S}$, where $x = (r - r_s^{m,n})/r_s^{m,n}$, $\nu_L = 1/2 - (1/4 + D)^{1/2}$, $\nu_S = 1/2 + (1/4 + D)^{1/2}$, and $D = [(2\,\mu_0\,P'/s^2\,B_\phi^2)]_{r_s^{m,n}}$, in the vicinity of a rational surface, $r = r_s^{m,n}$, at which $F^{m,n}(r_s^{m,n}) = 0$. Here, $s = r\,q'/q$. In fact, the correct result is $D = [(2\,\mu_0\,P'/s^2\,B_\phi^2)\,(1 - q^2)]_{r_s^{m,n}}$, where the additional multiplicative factor comes from the toroidal curvature of equilibrium magnetic field-lines.[4,30–32] Fortunately, this correction is irrelevant in RFPs, which are characterized by $q \ll 1$.

23 April 2024 14:39:08

© Author(s) 2024

III. STEPPED PRESSURE EQUILIBRIUM

A. Control surfaces

As is clear from Eqs. (55) and (56), including a continuous equilibrium pressure profile in our analysis leads to a great proliferation of additional terms in the linear eigenmode equation. One approach to simplifying the analysis is to approximate the equilibrium pressure profile as a stepped profile,[21,22] while still allowing the equilibrium parallel current profile to be smooth. Let us define the *control surfaces* $r = r_i$, for $i = 0, I+1$, where $r_i < r_{i+1}$ for $i = 0, I$, and $r_0 = 0$, $r_I = a$, $r_{I+1} = b$. Here, $I > 1$ is a positive integer, and b is the minor radius of a concentric perfectly conducting wall that surrounds the plasma. Suppose that the equilibrium pressure profile is such that $P(r) = P_i$, where P_i is a constant for $r_i < r < r_{i+1}$. Note that $P_I = 0$ (i.e., the pressure is zero in the vacuum region surrounding the plasma). According to Eq. (10), B_θ^2 and B_ϕ^2 are both discontinuous across the control surfaces. However, given that the safety-factor profile only depends on the parallel current profile [see Eq. (11)], which is smooth, the safety-factor profile must be continuous across the control surfaces, hence, making use of Eqs. (5) and (10),

$$\lim_{\delta\to 0}\left[B_\theta^2\right]_{r=r_i-\delta}^{r=r_i+\delta} = 2\,\mu_0\,(P_i - P_{i+1})\left(\frac{\epsilon^2}{\epsilon^2+q^2}\right)_{r=r_i}, \tag{57}$$

$$\lim_{\delta\to 0}\left[B_\phi^2\right]_{r=r_i-\delta}^{r=r_i+\delta} = 2\,\mu_0\,(P_i - P_{i+1})\left(\frac{q^2}{\epsilon^2+q^2}\right)_{r=r_i}, \tag{58}$$

for $i = 1, I$.

Between the control surfaces, Eqs. (8) and (9) reduce to

$$B_\phi' = -\frac{\sigma}{a}\,B_\theta, \tag{59}$$

$$B_\theta' + \frac{B_\theta}{r} = \frac{\sigma}{a}\,B_\phi. \tag{60}$$

Making use of Eqs. (5), (59), and (60), the safety-factor profile can determined from the parallel current profile by solving Eq. (11) subject to the boundary condition

$$q(0) = \frac{2\,\epsilon_a}{\sigma(0)}. \tag{61}$$

Furthermore, Eqs. (5) and (60) imply that

$$r\,B_\theta' = \left(\frac{\sigma\,q}{\epsilon_a} - 1\right)B_\theta, \tag{62}$$

between the control surfaces. We can solve this equation, subject to the boundary condition

$$\lim_{r\to 0}\left(\frac{B_\theta}{r}\right) = \frac{B_0}{q(0)\,R_0}, \tag{63}$$

where B_0 is the toroidal magnetic field-strength on the magnetic axis and also subject to the jump conditions (57) at the control surfaces. Once we have determined the equilibrium poloidal magnetic field profile, $B_\theta(r)$, the equilibrium toroidal magnetic field is specified by

$$B_\phi(r) = \frac{q\,B_\theta}{\epsilon}. \tag{64}$$

Finally, if we integrate the linear eigenmode equation (55) across each control surface, making use of Eqs. (8), (9), (21)–(23), (52), and (53), then we obtain

$$\lim_{\delta\to 0}\left[\psi_L^{m,n}\right]_{r=r_i-\delta}^{r=r_i+\delta} = 0, \tag{65}$$

$$\lim_{\delta\to 0}\left[r\,\frac{\partial\psi_L^{m,n}}{\partial r}\right]_{r=r_i-\delta}^{r=r_i+\delta} = J_i^{m,n}\,\psi_L^{m,n}(r_i,t), \tag{66}$$

for $i = 1, I$, where

$$J_i^{m,n} = K^{m,n}(r_i)\,\lim_{\delta\to 0}\frac{\left[B_\theta^2\right]_{r=r_i-\delta}^{r=r_i+\delta}}{B_\theta(r_i-\delta)\,B_\theta(r_i+\delta)}, \tag{67}$$

$$K^{m,n}(r) = \frac{1}{m-n\,q}\left[m + (m\,n\,q + n^2\,\epsilon^2)\left(\frac{\sigma}{2\,n\,\epsilon_a} - \frac{m}{m^2+n^2\,\epsilon^2}\right)\right] - \frac{(m\,n\,q+n^2\,\epsilon^2)}{(m-n\,q)^2}. \tag{68}$$

B. Simplified linear eigenmode equation

Between the control surfaces, the linear eigenmode equation, (55), takes a greatly simplified form in which[18]

$$g^{m,n}(r) = \frac{1}{r} + \frac{2\,m\,n\,\epsilon}{(H^{m,n})^2}\,\frac{\sigma}{a} - \frac{r}{H^{m,n}}\left(\frac{\sigma}{a}\right)^2 + \frac{r\,G^{m,n}}{H^{m,n}\,F^{m,n}}\,\frac{\sigma'}{a}. \tag{69}$$

[See Eq. (56).]

As is clear from Eqs. (52) and (69), the simplified linear eigenmode equation is singular at the equilibrium magnetic flux-surface, $r = r_s^{m,n}$, at which

$$F^{m,n}(r_s^{m,n}) = 0, \tag{70}$$

assuming that $0 < r_s^{m,n} < a$. It follows from Eqs. (5) and (21) that the safety-factor takes the rational value,

$$q(r_s^{m,n}) = \frac{m}{n}, \tag{71}$$

at the so-called (m, n) rational surface. The singular behavior of the linear eigenmode equation at the rational surface is indicative of a breakdown of the perturbed force balance relation, (12), in the immediate vicinity of the surface, and is ultimately resolved by incorporating plasma inertia, resistivity, and viscosity into the analysis.[27]

The most general solution of the simplified linear eigenmode equation in the immediate vicinity of the (m, n) rational surface is[27]

$$\psi_L^{m,n}(x,t) = C_l^{m,n}(t)\left[1 + \lambda^{m,n}\,x\,(\ln|x| - 1) + \mathcal{O}(x^2\,\ln|x|)\right] + C_s^{m,n}(t)\left[x + \mathcal{O}(x^2)\right], \tag{72}$$

where

$$x = \frac{r - r_s^{m,n}}{r_s^{m,n}}, \tag{73}$$

$$\lambda^{m,n} = \left[\frac{r\,G^{m,n}}{(F^{m,n})'}\,\frac{\sigma'}{a}\right]_{r=r_s^{m,n}}. \tag{74}$$

(Note that the Mercier indices take the simplified values $\nu_L = 0$ and $\nu_S = 1$ on rational surfaces lying between the control surfaces.) Here,

23 April 2024 14:39:08

© Author(s) 2024

$C_l^{m,n}$ and $C_s^{m,n}$ are known as the coefficients of the large and small solutions, respectively.

As is well known, if we neglect twisting parity modes, as is reasonable,[29] the coefficient of the large solution must be continuous across the (m, n) rational surface, whereas the coefficient of the small solutions may be discontinuous.[27–29,33] The discontinuity in the coefficient of the small solution is associated with a helical current sheet (with m periods in θ, and n periods in ϕ) that flows parallel to the equilibrium magnetic field in the immediate vicinity of the rational surface. Thus, the (m, n) linear eigenmode can be characterized by the following two complex parameters:[28]

$$\Psi^{m,n}(t) = \frac{C_l^{m,n}(t)}{\left[H^{m,n}(r_s^{m,n})\right]^{1/2}}, \tag{75}$$

$$\Delta\Psi^{m,n}(t) = \frac{\lim_{\delta\to 0}\left[C_s^{m,n}(t)\right]_{r=r_s^{m,n}-\delta}^{r=r_s^{m,n}+\delta}}{\left[H^{m,n}(r_s^{m,n})\right]^{1/2}}. \tag{76}$$

Here, $\Psi^{m,n}(t)$ is the reconnected helical magnetic flux (divided by $\pi^2 R_0$) at the (m, n) rational surface, whereas $\Delta\Psi^{m,n}(t)$ parameterizes the amplitude and phase of the current sheet.

Let

$$\psi_L^{m,n}(r,t) = \Psi^{m,n}(t)\,\hat{\psi}^{m,n}(r), \tag{77}$$

where $\hat{\psi}^{m,n}(r)$ is a real solution of

$$\frac{d}{dr}\left(f^{m,n}\,\frac{d\hat{\psi}^{m,n}}{dr}\right) - g^{m,n}\,\hat{\psi}^{m,n} = 0 \tag{78}$$

[see Eq. (55)], with $f^{m,n}(r)$ and $g^{m,n}(r)$ specified by Eqs. (52) and (69), respectively, that is continuous across the (m, n) rational surface, is subject to the normalization constraint

$$\hat{\psi}^{m,n}(r_s^{m,n}) = 1, \tag{79}$$

and satisfies the jump conditions

$$\lim_{\delta\to 0}\left[\hat{\psi}^{m,n}\right]_{r=r_i-\delta}^{r=r_i+\delta} = 0, \tag{80}$$

$$\lim_{\delta\to 0}\left[r\,\frac{d\hat{\psi}^{m,n}}{dr}\right]_{r=r_i-\delta}^{r=r_i+\delta} = J_i^{m,n}\,\hat{\psi}^{m,n}(r_i), \tag{81}$$

for $i = 1, I$, at the control surfaces [see Eqs. (65) and (66)].

When written in terms of $\Psi^{m,n}(t)$ and $\hat{\psi}^{m,n}(r)$, the linearized magnetic field and plasma current density perturbations associated with an (m, n) tearing mode take the forms [see Eqs. (21)–(23), (31)–(36), (59), and (60)][18]

$$b_{rL}^{m,n}(r,t) = \mathrm{i}\,\Psi^{m,n}(t)\,\hat{b}_r^{m,n}(r), \tag{82}$$

$$b_{\theta L}^{m,n}(r,t) = \Psi^{m,n}(t)\,\hat{b}_\theta^{m,n}(r), \tag{83}$$

$$b_{\phi L}^{m,n}(r,t) = \Psi^{m,n}(t)\,\hat{b}_\phi^{m,n}(r), \tag{84}$$

$$\mu_0 j_{rL}^{m,n}(r,t) = \mathrm{i}\,\Psi^{m,n}(t)\,\hat{j}_r^{m,n}(r), \tag{85}$$

$$\mu_0 j_{\theta L}^{m,n}(r,t) = \Psi^{m,n}(t)\,\hat{j}_\theta^{m,n}(r), \tag{86}$$

$$\mu_0 j_{\phi L}^{m,n}(r,t) = \Psi^{m,n}(t)\,\hat{j}_\phi^{m,n}(r), \tag{87}$$

where[18]

$$\hat{b}_r^{m,n}(r) = \frac{\hat{\psi}^{m,n}}{r}, \tag{88}$$

$$\hat{b}_\theta^{m,n}(r) = -\frac{m}{H^{m,n}}\left(\hat{\psi}^{m,n}\right)' + \frac{n\,\epsilon}{H^{m,n}}\,\frac{\sigma}{a}\,\hat{\psi}^{m,n}, \tag{89}$$

$$\hat{b}_\phi^{m,n}(r) = \frac{n\,\epsilon}{H^{m,n}}\left(\hat{\psi}^{m,n}\right)' + \frac{m}{H^{m,n}}\,\frac{\sigma}{a}\,\hat{\psi}^{m,n}, \tag{90}$$

$$\hat{j}_r^{m,n}(r) = \frac{\sigma}{a}\,\frac{\hat{\psi}^{m,n}}{r}, \tag{91}$$

$$\hat{j}_\theta^{m,n}(r) = \frac{\sigma}{a}\left[-\frac{m}{H^{m,n}}\left(\hat{\psi}^{m,n}\right)' + \frac{n\,\epsilon}{H^{m,n}}\,\frac{\sigma}{a}\,\hat{\psi}^{m,n}\right] - \frac{B_\theta}{F^{m,n}}\,\frac{\sigma'}{a}\,\hat{\psi}^{m,n}, \tag{92}$$

$$\hat{j}_\phi^{m,n}(r) = \frac{\sigma}{a}\left[\frac{n\,\epsilon}{H^{m,n}}\left(\hat{\psi}^{m,n}\right)' + \frac{m}{H^{m,n}}\,\frac{\sigma}{a}\,\hat{\psi}^{m,n}\right] - \frac{B_\phi}{F^{m,n}}\,\frac{\sigma'}{a}\,\hat{\psi}^{m,n}. \tag{93}$$

C. Spatial boundary conditions

Close to the magnetic axis (i.e., $r \to 0$), the normalized linear eigenmode equation, (78), reduces to

$$r\,\frac{d}{dr}\left(r\,\frac{d\hat{\psi}^{m,n}}{dr}\right) - m^2\,\hat{\psi}^{m,n} = 0. \tag{94}$$

Here, use has been made of Eqs. (52) and (69), as well as the fact that σ, $H^{m,n}$, $G^{m,n} \propto r^0$, and σ', $F^{m,n} \propto r$, as $r \to 0$. Thus, the solution that is well behaved at the magnetic axis satisfies the boundary condition

$$\left(\frac{d\ln\hat{\psi}^{m,n}}{d\ln r}\right)_{r=0} = |m|. \tag{95}$$

However, for the special case $m = 0$, $H^{m,n} \propto r^2$, and the boundary condition becomes

$$\left(\frac{d\ln\hat{\psi}^{0,n}}{d\ln r}\right)_{r=0} = 2. \tag{96}$$

In the vacuum region outside the plasma, $r > a$ (where $\sigma = 0$), the normalized linear eigenmode equation, (78), reduces to

$$r\,\frac{d}{dr}\left(\frac{r}{m^2+n^2\,\epsilon^2}\,\frac{d\hat{\psi}^{m,n}}{dr}\right) - \hat{\psi}^{m,n} = 0, \tag{97}$$

where use has been made of Eqs. (23), (52), and (69). Let

$$\chi^{m,n}(r) = \frac{r}{m^2+n^2\,\epsilon^2}\,\frac{d\hat{\psi}^{m,n}}{dr}. \tag{98}$$

It follows from Eq. (97) that:

$$\hat{\psi}^{m,n}(r) = r\,\frac{d\chi^{m,n}}{dr}, \tag{99}$$

and

$$z^2\,\frac{d^2\chi^{m,n}}{dz^2} + z\,\frac{d\chi^{m,n}}{dz} - (m^2+z^2)\,\chi^{m,n} = 0, \tag{100}$$

23 April 2024 14:39:08

© Author(s) 2024

where $z = n\,\epsilon$. The physical boundary condition at the perfectly conducting wall surrounding the plasma is

$$b_{rL}^{m,n}(b,t) = 0, \tag{101}$$

which, from Eqs. (82) and (88), implies that

$$\hat{\psi}^{m,n}(b) = 0. \tag{102}$$

It follows from Eq. (99) that

$$\frac{d\chi^{m,n}(b)}{dr} = 0. \tag{103}$$

Hence, according to Eq. (100), in the vacuum region surrounding the plasma ($a \leq r \leq b$),

$$\chi^{m,n}(r) = A\left[I_m(n\,\epsilon)\,K_m'(n\,\epsilon_b) - K_m(n\,\epsilon)\,I_m'(n\,\epsilon_b)\right], \tag{104}$$

where $I_m(z)$, $K_m(z)$ are modified Bessel functions, $I_m'(z) = dI_m/dz$, $K_m'(z) = dK_m/dz$, $\epsilon_b = b/R_0$, and A is an arbitrary constant. Equation (99) yields

$$\hat{\psi}^{m,n}(r) = A\,n\,\epsilon\left[I_m'(n\,\epsilon)\,K_m'(n\,\epsilon_b) - K_m'(n\,\epsilon)\,I_m'(n\,\epsilon_b)\right]. \tag{105}$$

The previous two equations can be combined with Eq. (98) to give the following boundary condition at the edge of the plasma:

$$\left(\frac{d\ln\hat{\psi}^{m,n}}{d\ln r}\right)_{r=a} = \frac{m^2 + n^2\,\epsilon_a^2}{n\,\epsilon_a}\frac{I_m(n\,\epsilon_a)\,K_m'(n\,\epsilon_b) - K_m(n\,\epsilon_a)\,I_m'(n\,\epsilon_b)}{I_m'(n\,\epsilon_a)\,K_m'(n\,\epsilon_b) - K_m'(n\,\epsilon_a)\,I_m'(n\,\epsilon_b)}. \tag{106}$$

The continuous solution of the normalized linear eigenmode equation, (78), that satisfies the boundary conditions (95) and (106), as well as the normalizing constraint (79), and the jump conditions (80) and (81), is unique, and, in general, possesses a gradient discontinuity at the (m, n) rational surface. This discontinuity is conveniently parameterized by the real dimensionless parameter[27,28]

$$\Delta^{m,n} = \left[r\,\frac{d\hat{\psi}^{m,n}}{dr}\right]_{r=r_s^{m,n}-}^{r=r_s^{m,n}+}. \tag{107}$$

According to conventional analysis, the (m, n) tearing mode is unstable when $\Delta^{m,n} > 0$ and is stable otherwise.[27,34] Moreover, an unstable tearing mode eventually saturates at an amplitude that is such that the width of the magnetic island chain [see Eq. (175)] that forms at the rational surface is roughly proportional to $\Delta^{m,n}$.[35–39] Note that if there is no (m, n) rational surface in the plasma, then the only solution to Eq. (78) that satisfies the boundary conditions (95) and (106) is $\hat{\psi}^{m,n}(r) = 0$ for $0 \leq r \leq a$.

IV. NONLINEAR MODE COUPLING THEORY

A. Nonlinear coupling coefficients

Consider the nonlinear coupling of three tearing modes with poloidal and toroidal mode numbers (m_1, n_1), and (m_2, n_2), and (m_3, n_3), where

$$m_3 = m_1 + m_2, \tag{108}$$

$$n_3 = n_1 + n_2. \tag{109}$$

Let us calculate the various nonlinear coupling coefficients from Eq. (17) using the linear eigenfunctions.

Making use of Eqs. (17) and (82)–(87),

$$\begin{aligned} A_r^{m_3,n_3}(r,t) = \frac{1}{2}\,\Psi^{m_1,n_1}\,\Psi^{m_2,n_2}\Bigg[&- \hat{b}_r^{m_1,n_1}\,\frac{d\hat{j}_r^{m_2,n_2}}{dr} - \hat{b}_r^{m_2,n_2}\,\frac{d\hat{j}_r^{m_1,n_1}}{dr} + \hat{j}_r^{m_1,n_1}\,\frac{d\hat{b}_r^{m_2,n_2}}{dr} \\ &+ \hat{j}_r^{m_2,n_2}\,\frac{d\hat{b}_r^{m_1,n_1}}{dr} - \hat{b}_\theta^{m_1,n_1}\,\frac{m_2}{r}\,\hat{j}_r^{m_2,n_2} - \hat{b}_\theta^{m_2,n_2}\,\frac{m_1}{r}\,\hat{j}_r^{m_1,n_1} + \hat{j}_\theta^{m_1,n_1}\,\frac{m_2}{r}\,\hat{b}_r^{m_2,n_2} \\ &+ \hat{j}_\theta^{m_2,n_2}\,\frac{m_1}{r}\,\hat{b}_r^{m_1,n_1} + \hat{b}_\phi^{m_1,n_1}\,\frac{n_2\,\epsilon}{r}\,\hat{j}_r^{m_2,n_2} + \hat{b}_\phi^{m_2,n_2}\,\frac{n_1\,\epsilon}{r}\,\hat{j}_r^{m_1,n_1} - \hat{j}_\phi^{m_1,n_1}\,\frac{n_2\,\epsilon}{r}\,\hat{b}_r^{m_2,n_2} - \hat{j}_\phi^{m_2,n_2}\,\frac{n_1\,\epsilon}{r}\,\hat{b}_r^{m_1,n_1}\Bigg]. \end{aligned} \tag{110}$$

Hence, it follows from Eqs. (88)–(93) that[18]

$$A_r^{m_3,n_3}(r,t) = -\frac{1}{2}\,\Psi^{m_1,n_1}\,\Psi^{m_2,n_2}\,\frac{\sigma'}{a}\,\frac{\hat{\psi}^{m_1,n_1}\,\hat{\psi}^{m_2,n_2}}{r^2}\,\frac{(F^{m_3,n_3})^2}{F^{m_1,n_1}\,F^{m_2,n_2}}. \tag{111}$$

Analogous calculations reveal that

$$A_r^{m_1,n_1}(r,t) = -\frac{1}{2}\,(\Psi^{m_2,n_2})^*\,\Psi^{m_3,n_3}\,\frac{\sigma'}{a}\,\frac{\hat{\psi}^{m_2,n_2}\,\hat{\psi}^{m_3,n_3}}{r^2}\,\frac{(F^{m_1,n_1})^2}{F^{m_2,n_2}\,F^{m_3,n_3}}, \tag{112}$$

$$A_r^{m_2,n_2}(r,t) = -\frac{1}{2}\,\Psi^{m_3,n_3}\,(\Psi^{m_1,n_1})^*\,\frac{\sigma'}{a}\,\frac{\hat{\psi}^{m_3,n_3}\,\hat{\psi}^{m_1,n_1}}{r^2}\,\frac{(F^{m_2,n_2})^2}{F^{m_3,n_3}\,F^{m_1,n_1}}. \tag{113}$$

Making use of Eqs. (17) and (82)–(87),

23 April 2024 14:39:08

© Author(s) 2024

$$A_\theta^{m_3,n_3}(r,t) = \frac{1}{2}\,\Psi^{m_1,n_1}\,\Psi^{m_2,n_2}\,\mathrm{i}\Big[\hat{b}_r^{m_1,n_1}\,r\,\frac{d(\hat{j}_\theta^{m_2,n_2}/r)}{dr} + \hat{b}_r^{m_2,n_2}\,r\,\frac{d(\hat{j}_\theta^{m_1,n_1}/r)}{dr} - \hat{j}_r^{m_1,n_1}\,r\,\frac{d(\hat{b}_\theta^{m_2,n_2}/r)}{dr} - \hat{j}_r^{m_2,n_2}\,r\,\frac{d(\hat{b}_\theta^{m_1,n_1}/r)}{dr}$$
$$+ \hat{b}_\theta^{m_1,n_1}\,\frac{m_2}{r}\,\hat{j}_\theta^{m_2,n_2} + \hat{b}_\theta^{m_2,n_2}\,\frac{m_1}{r}\,\hat{j}_\theta^{m_1,n_1} - \hat{j}_\theta^{m_1,n_1}\,\frac{m_2}{r}\,\hat{b}_\theta^{m_2,n_2} - \hat{j}_\theta^{m_2,n_2}\,\frac{m_1}{r}\,\hat{b}_\theta^{m_1,n_1} - \hat{b}_\phi^{m_1,n_1}\,\frac{n_2\,\epsilon}{r}\,\hat{j}_\theta^{m_2,n_2}$$
$$- \hat{b}_\phi^{m_2,n_2}\,\frac{n_1\,\epsilon}{r}\,\hat{j}_\theta^{m_1,n_1} + \hat{j}_\phi^{m_1,n_1}\,\frac{n_2\,\epsilon}{r}\,\hat{b}_\theta^{m_2,n_2} + \hat{j}_\phi^{m_2,n_2}\,\frac{n_1\,\epsilon}{r}\,\hat{b}_\theta^{m_1,n_1}\Big]. \tag{114}$$

Hence, it follows from Eqs. (88)–(93) that[18]

$$A_\theta^{m_3,n_3}(r,t) = \frac{1}{2}\,\Psi^{m_1,n_1}\,\Psi^{m_2,n_2}\,\mathrm{i}\Big[\frac{\sigma'}{a}\,\frac{\hat{\psi}^{m_1,n_1}\,(\hat{\psi}^{m_2,n_2})'}{r}\,\frac{n_3\,\epsilon\,G^{m_2,n_2}}{H^{m_2,n_2}\,F^{m_1,n_1}} + \frac{\sigma'}{a}\,\frac{\hat{\psi}^{m_2,n_2}\,(\hat{\psi}^{m_1,n_1})'}{r}\,\frac{n_3\,\epsilon\,G^{m_1,n_1}}{H^{m_1,n_1}\,F^{m_2,n_2}}$$
$$+ \frac{\sigma'}{a}\,\frac{\sigma}{a}\,\frac{n_3\,\epsilon\,\hat{\psi}^{m_1,n_1}\,\hat{\psi}^{m_2,n_2}}{r}\left(\frac{F^{m_1,n_1}}{H^{m_1,n_1}\,F^{m_2,n_2}} + \frac{F^{m_2,n_2}}{H^{m_2,n_2}\,F^{m_1,n_1}}\right) - \left(\frac{\sigma'}{a}\,\frac{\hat{\psi}^{m_1,n_2}\,\hat{\psi}^{m_2,n_2}}{r}\,\frac{B_\theta\,F^{m_3,n_3}}{F^{m_1,n_1}\,F^{m_2,n_2}}\right)'\Big]. \tag{115}$$

Analogous calculations reveal that

$$A_\theta^{m_1,n_1}(r,t) = \frac{1}{2}\,(\Psi^{m_2,n_2})^*\,\Psi^{m_3,n_3}\,\mathrm{i}\Big[\frac{\sigma'}{a}\,\frac{\hat{\psi}^{m_2,n_2}\,(\hat{\psi}^{m_3,n_3})'}{r}\,\frac{n_1\,\epsilon\,G^{m_3,n_3}}{H^{m_3,n_3}\,F^{m_2,n_2}} + \frac{\sigma'}{a}\,\frac{\hat{\psi}^{m_3,n_3}\,(\hat{\psi}^{m_2,n_2})'}{r}\,\frac{n_1\,\epsilon\,G^{m_2,n_2}}{H^{m_2,n_2}\,F^{m_3,n_3}}$$
$$+ \frac{\sigma'}{a}\,\frac{\sigma}{a}\,\frac{n_1\,\epsilon\,\hat{\psi}^{m_2,n_2}\,\hat{\psi}^{m_3,n_3}}{r}\left(\frac{F^{m_2,n_2}}{H^{m_2,n_2}\,F^{m_3,n_3}} + \frac{F^{m_3,n_3}}{H^{m_3,n_3}\,F^{m_2,n_2}}\right) - \left(\frac{\sigma'}{a}\,\frac{\hat{\psi}^{m_2,n_2}\,\hat{\psi}^{m_3,n_3}}{r}\,\frac{B_\theta\,F^{m_1,n_1}}{F^{m_2,n_2}\,F^{m_3,n_3}}\right)'\Big], \tag{116}$$

and

$$A_\theta^{m_2,n_2}(r,t) = \frac{1}{2}\,(\Psi^{m_1,n_1})^*\,\Psi^{m_3,n_3}\,\mathrm{i}\Big[\frac{\sigma'}{a}\,\frac{\hat{\psi}^{m_3,n_3}\,(\hat{\psi}^{m_1,n_1})'}{r}\,\frac{n_2\,\epsilon\,G^{m_1,n_1}}{H^{m_1,n_1}\,F^{m_3,n_3}} + \frac{\sigma'}{a}\,\frac{\hat{\psi}^{m_1,n_1}\,(\hat{\psi}^{m_3,n_3})'}{r}\,\frac{n_2\,\epsilon\,G^{m_3,n_3}}{H^{m_3,n_3}\,F^{m_1,n_1}}$$
$$+ \frac{\sigma'}{a}\,\frac{\sigma}{a}\,\frac{n_2\,\epsilon\,\hat{\psi}^{m_3,n_3}\,\hat{\psi}^{m_1,n_1}}{r}\left(\frac{F^{m_3,n_3}}{H^{m_3,n_3}\,F^{m_1,n_1}} + \frac{F^{m_1,n_1}}{H^{m_1,n_1}\,F^{m_3,n_3}}\right) - \left(\frac{\sigma'}{a}\,\frac{\hat{\psi}^{m_3,n_3}\,\hat{\psi}^{m_1,n_1}}{r}\,\frac{B_\theta\,F^{m_2,n_2}}{F^{m_3,n_3}\,F^{m_1,n_1}}\right)'\Big]. \tag{117}$$

Making use of Eqs. (17) and (82)–(87),

$$A_\phi^{m_3,n_3}(r,t) = \frac{1}{2}\,\Psi^{m_1,n_1}\,\Psi^{m_2,n_2}\,\mathrm{i}\Big[\hat{b}_r^{m_1,n_1}\,\frac{d\hat{j}_\phi^{m_2,n_2}}{dr} + \hat{b}_r^{m_2,n_2}\,\frac{d\hat{j}_\phi^{m_1,n_1}}{dr} - \hat{j}_r^{m_1,n_1}\,\frac{d\hat{b}_\phi^{m_2,n_2}}{dr} - \hat{j}_r^{m_2,n_2}\,\frac{d\hat{b}_\phi^{m_1,n_1}}{dr} + \hat{b}_\theta^{m_1,n_1}\,\frac{m_2}{r}\,\hat{j}_\phi^{m_2,n_2}$$
$$+ \hat{b}_\theta^{m_2,n_2}\,\frac{m_1}{r}\,\hat{j}_\phi^{m_1,n_1} - \hat{j}_\theta^{m_1,n_1}\,\frac{m_2}{r}\,\hat{b}_\phi^{m_2,n_2} - \hat{j}_\theta^{m_2,n_2}\,\frac{m_1}{r}\,\hat{b}_\phi^{m_1,n_1} - \hat{b}_\phi^{m_1,n_1}\,\frac{n_2\,\epsilon}{r}\,\hat{j}_\phi^{m_2,n_2} - \hat{b}_\phi^{m_2,n_2}\,\frac{n_1\,\epsilon}{r}\,\hat{j}_\phi^{m_1,n_1}$$
$$+ \hat{j}_\phi^{m_1,n_1}\,\frac{n_2\,\epsilon}{r}\,\hat{b}_\phi^{m_2,n_2} + \hat{j}_\phi^{m_2,n_2}\,\frac{n_1\,\epsilon}{r}\,\hat{b}_\phi^{m_1,n_1}\Big]. \tag{118}$$

Hence, it follows from Eqs. (88)–(93) that[18]

$$A_\phi^{m_3,n_3}(r,t) = \frac{1}{2}\,\Psi^{m_1,n_1}\,\Psi^{m_2,n_2}\,\mathrm{i}\Big[\frac{\sigma'}{a}\,\frac{\hat{\psi}^{m_1,n_1}\,(\hat{\psi}^{m_2,n_2})'}{r}\,\frac{m_3\,G^{m_2,n_2}}{H^{m_2,n_2}\,F^{m_1,n_1}} + \frac{\sigma'}{a}\,\frac{\hat{\psi}^{m_2,n_2}\,(\hat{\psi}^{m_1,n_1})'}{r}\,\frac{m_3\,G^{m_1,n_1}}{H^{m_1,n_1}\,F^{m_2,n_2}}$$
$$+ \frac{\sigma'}{a}\,\frac{\sigma}{a}\,\frac{m_3\,\hat{\psi}^{m_1,n_1}\,\hat{\psi}^{m_2,n_2}}{r}\left(\frac{F^{m_1,n_1}}{H^{m_1,n_1}\,F^{m_2,n_2}} + \frac{F^{m_2,n_2}}{H^{m_2,n_2}\,F^{m_1,n_1}}\right) - \frac{1}{r}\left(\frac{\sigma'}{a}\,\hat{\psi}^{m_1,n_1}\,\hat{\psi}^{m_2,n_2}\,\frac{B_\phi\,F^{m_3,n_3}}{F^{m_1,n_1}\,F^{m_2,n_2}}\right)'\Big]. \tag{119}$$

Analogous calculations reveal that

$$A_\phi^{m_1,n_1}(r,t) = \frac{1}{2}\,(\Psi^{m_2,n_2})^*\,\Psi^{m_3,n_3}\,\mathrm{i}\Big[\frac{\sigma'}{a}\,\frac{\hat{\psi}^{m_2,n_2}\,(\hat{\psi}^{m_3,n_3})'}{r}\,\frac{m_1\,G^{m_3,n_3}}{H^{m_3,n_3}\,F^{m_2,n_2}} + \frac{\sigma'}{a}\,\frac{\hat{\psi}^{m_3,n_3}\,(\hat{\psi}^{m_2,n_2})'}{r}\,\frac{m_1\,G^{m_2,n_2}}{H^{m_2,n_2}\,F^{m_3,n_3}}$$
$$+ \frac{\sigma'}{a}\,\frac{\sigma}{a}\,\frac{m_1\,\hat{\psi}^{m_2,n_2}\,\hat{\psi}^{m_3,n_3}}{r}\left(\frac{F^{m_2,n_2}}{H^{m_2,n_2}\,F^{m_3,n_3}} + \frac{F^{m_3,n_3}}{H^{m_3,n_3}\,F^{m_2,n_2}}\right) - \frac{1}{r}\left(\frac{\sigma'}{a}\,\hat{\psi}^{m_2,n_2}\,\hat{\psi}^{m_3,n_3}\,\frac{B_\phi\,F^{m_1,n_1}}{F^{m_2,n_2}\,F^{m_3,n_3}}\right)'\Big], \tag{120}$$

and

23 April 2024 14:39:08

© Author(s) 2024

$$A_\phi^{m_2,n_2}(r,t) = \frac{1}{2}\,\Psi^{m_3,n_3}\,(\Psi^{m_1,n_1})^*\,\mathrm{i}\left[\frac{\sigma'}{a}\,\frac{\hat\psi^{m_3,n_3}\,(\hat\psi^{m_1,n_1})'}{r}\,\frac{m_2\,G^{m_1,n_1}}{H^{m_1,n_1}\,F^{m_3,n_3}} + \frac{\sigma'}{a}\,\frac{\hat\psi^{m_1,n_1}\,(\hat\psi^{m_3,n_3})'}{r}\,\frac{m_2\,G^{m_3,n_3}}{H^{m_3,n_3}\,F^{m_1,n_1}}\right.$$
$$\left. + \frac{\sigma'}{a}\,\frac{\sigma}{a}\,\frac{m_2\,\hat\psi^{m_3,n_3}\,\hat\psi^{m_1,n_1}}{r}\left(\frac{F^{m_3,n_3}}{H^{m_3,n_3}\,F^{m_1,n_1}} + \frac{F^{m_1,n_1}}{H^{m_1,n_1}\,F^{m_3,n_3}}\right) - \frac{1}{r}\left(\frac{\sigma'}{a}\,\hat\psi^{m_3,n_3}\,\hat\psi^{m_1,n_1}\,\frac{B_\phi\,F^{m_2,n_2}}{F^{m_3,n_3}\,F^{m_1,n_1}}\right)'\right]. \tag{121}$$

Note that the nonlinear coupling coefficients are all zero in the vacuum region surrounding the plasma (where $\sigma' = 0$). This is to be expected because the nonlinear coupling is generated by the $\mathbf{j}\times\mathbf{b}$ force density, and $\mathbf{j} = \mathbf{0}$ in a vacuum.

Finally, it is easily verified, from Eqs. (111)–(113), (115)–(117), and (119)–(121), that the self-consistency constraint (28) is separately satisfied for $(m,n) = (m_1,n_1)$ or (m_2,n_2) or (m_3,n_3).

B. Electromagnetic torques

The flux-surface integrated poloidal electromagnetic torque acting on the plasma can be written as

$$T_\theta(r,t) = \oint\!\!\oint\!\!\int r\,[(\mathbf{J}+\mathbf{j})\times(\mathbf{B}+\mathbf{b})]\cdot\mathbf{e}_\theta\,r\,d\theta\,R_0\,d\phi$$
$$= R_0\oint\!\!\oint\!\!\int r^2\,\mathbf{j}\times\mathbf{b}\cdot\mathbf{e}_\theta\,d\theta\,d\phi$$
$$= \frac{\pi^2\,R_0}{\mu_0}\,\frac{\partial}{\partial r}\left[\sum_{m,n} X_\theta^{m,n}(r,t)\right], \tag{122}$$

where

$$X_\theta^{m,n}(r,t) = r^2\left[b_r^{m,n}\,(b_\theta^{m,n})^* + (b_r^{m,n})^*\,b_\theta^{m,n}\right], \tag{123}$$

and use has been made Eqs. (13), (14), and (19). Note that equilibrium terms make no contribution to the torque. Moreover, linear terms average to zero over a flux-surface. Hence, we are just left with nonlinear terms. Likewise, the flux-surface integrated toroidal electromagnetic torque acting on the plasma can be written as

$$T_\phi(r,t) = \oint\!\!\oint\!\!\int R_0\,[(\mathbf{J}+\mathbf{j})\times(\mathbf{B}+\mathbf{b})]\cdot\mathbf{e}_\phi\,r\,d\theta\,R_0\,d\phi$$
$$= R_0^2\oint\!\!\oint\!\!\int r\,\mathbf{j}\times\mathbf{b}\cdot\mathbf{e}_\phi\,d\theta\,d\phi$$
$$= -\frac{\pi^2\,R_0}{\mu_0}\,\frac{\partial}{\partial r}\left[\sum_{m,n} X_\phi^{m,n}(r,t)\right], \tag{124}$$

where

$$X_\phi^{m,n}(r,t) = -r\,R_0\left[b_r^{m,n}\,(b_\phi^{m,n})^* + (b_r^{m,n})^*\,b_\phi^{m,n}\right]. \tag{125}$$

Making use of Eqs. (23), (31)–(33), and (52), we find that

$$X_\theta^{m,n}(r,t) = \mathrm{i}\left[m f^{m,n}\,\frac{\partial\psi^{m,n}}{\partial r}\,(\psi^{m,n})^* - \frac{n\,\epsilon\,r^3\,A_r^{m,n}\,(\psi^{m,n})^*}{H^{m,n}\,F^{m,n}}\right] + \text{c.c.}, \tag{126}$$

$$X_\phi^{m,n}(r,t) = \mathrm{i}\left[n f^{m,n}\,\frac{\partial\psi^{m,n}}{\partial r}\,(\psi^{m,n})^* + \frac{m\,r^2\,R_0\,A_r^{m,n}\,(\psi^{m,n})^*}{H^{m,n}\,F^{m,n}}\right] + \text{c.c.}. \tag{127}$$

Thus, it follows from Eq. (51) that

$$\frac{\partial X_\theta}{\partial r} = \mathrm{i}\,m\,V^{m,n}\,(\psi^{m,n})^* - \mathrm{i}\,\frac{\partial}{\partial r}\left[\frac{n\,\epsilon\,r^3\,A_r^{m,n}\,(\psi^{m,n})^*}{H^{m,n}\,F^{m,n}}\right] + \text{c.c.}, \tag{128}$$

$$\frac{\partial X_\phi}{\partial r} = \mathrm{i}\,n\,V^{m,n}\,(\psi^{m,n})^* + \mathrm{i}\,\frac{\partial}{\partial r}\left[\frac{m\,r^2\,R_0\,A_r^{m,n}\,(\psi^{m,n})^*}{H^{m,n}\,F^{m,n}}\right] + \text{c.c.}. \tag{129}$$

Here, we have made use of the fact that $f^{m,n}(r)$ and $g^{m,n}(r)$ are real functions.

Making use of Eqs. (54), (77), (111)–(113), (115)–(117), and (119)–(121), the previous two equations yield[18]

$$\frac{\partial X_\theta^{m_1,n_1}}{\partial r} = \mathrm{Im}\left[(\Psi^{m_1,n_1}\,\Psi^{m_2,n_2})^*\,\Psi^{m_3,n_3}\right]$$
$$\times\left[-m_1\,\tau + \left(\frac{\sigma'}{a}\,\frac{\hat\psi^{m_1,n_1}\,\hat\psi^{m_2,n_2}\,\hat\psi^{m_3,n_3}\,r\,B_\phi}{F^{m_2,n_2}\,F^{m_3,n_3}}\right)'\right], \tag{130}$$

$$\frac{\partial X_\theta^{m_2,n_2}}{\partial r} = \mathrm{Im}\left[(\Psi^{m_1,n_1}\,\Psi^{m_2,n_2})^*\,\Psi^{m_3,n_3}\right]$$
$$\times\left[-m_2\,\tau + \left(\frac{\sigma'}{a}\,\frac{\hat\psi^{m_1,n_1}\,\hat\psi^{m_2,n_2}\,\hat\psi^{m_3,n_3}\,r\,B_\phi}{F^{m_1,n_1}\,F^{m_3,n_3}}\right)'\right], \tag{131}$$

$$\frac{\partial X_\theta^{m_3,n_3}}{\partial r} = \mathrm{Im}\left[(\Psi^{m_1,n_1}\,\Psi^{m_2,n_2})^*\,\Psi^{m_3,n_3}\right]$$
$$\times\left[m_3\,\tau - \left(\frac{\sigma'}{a}\,\frac{\hat\psi^{m_1,n_1}\,\hat\psi^{m_2,n_2}\,\hat\psi^{m_3,n_3}\,r\,B_\phi}{F^{m_1,n_1}\,F^{m_2,n_2}}\right)'\right], \tag{132}$$

and

$$\frac{\partial X_\phi^{m_1,n_1}}{\partial r} = \mathrm{Im}\left[(\Psi^{m_1,n_1}\,\Psi^{m_2,n_2})^*\,\Psi^{m_3,n_3}\right]$$
$$\times\left[-n_1\,\tau + \left(\frac{\sigma'}{a}\,\frac{\hat\psi^{m_1,n_1}\,\hat\psi^{m_2,n_2}\,\hat\psi^{m_3,n_3}\,r\,B_\theta}{\epsilon\,F^{m_2,n_2}\,F^{m_3,n_3}}\right)'\right], \tag{133}$$

$$\frac{\partial X_\phi^{m_2,n_2}}{\partial r} = \mathrm{Im}\left[(\Psi^{m_1,n_1}\,\Psi^{m_2,n_2})^*\,\Psi^{m_3,n_3}\right]$$
$$\times\left[-n_2\,\tau + \left(\frac{\sigma'}{a}\,\frac{\hat\psi^{m_1,n_1}\,\hat\psi^{m_2,n_2}\,\hat\psi^{m_3,n_3}\,r\,B_\theta}{\epsilon\,F^{m_1,n_1}\,F^{m_3,n_3}}\right)'\right], \tag{134}$$

23 April 2024 14:39:08

© Author(s) 2024

$$\frac{\partial X_\phi^{m_3,n_3}}{\partial r} = \mathrm{Im}\left[(\Psi^{m_1,n_1}\,\Psi^{m_2,n_2})^*\,\Psi^{m_3,n_3}\right] \times\left[n_3\,\tau - \left(\frac{\sigma'}{a}\frac{\hat\psi^{m_1,n_1}\,\hat\psi^{m_2,n_2}\,\hat\psi^{m_3,n_3}\,r\,B_\theta}{\epsilon\,F^{m_1,n_1}\,F^{m_2,n_2}}\right)'\right], \tag{135}$$

where[18]

$$\begin{aligned}\tau(r) = \frac{\sigma'}{a}\Bigg\{ & r\,(\hat\psi^{m_1,n_1})'\,\hat\psi^{m_2,n_2}\,\hat\psi^{m_3,n_3}\,\frac{G^{m_1,n_1}}{H^{m_1,n_1}\,F^{m_2,n_2}\,F^{m_3,n_3}}\\ & + r\,(\hat\psi^{m_2,n_2})'\,\hat\psi^{m_3,n_3}\,\hat\psi^{m_1,n_1}\,\frac{G^{m_2,n_2}}{H^{m_2,n_2}\,F^{m_3,n_3}\,F^{m_1,n_1}}\\ & + r\,(\hat\psi^{m_3,n_3})'\,\hat\psi^{m_1,n_1}\,\hat\psi^{m_2,n_2}\,\frac{G^{m_3,n_3}}{H^{m_3,n_3}\,F^{m_1,n_1}\,F^{m_2,n_2}}\\ & + r\,\frac{\sigma}{a}\,\hat\psi^{m_1,n_1}\,\hat\psi^{m_2,n_2}\,\hat\psi^{m_3,n_3}\left(\frac{F^{m_1,n_1}}{H^{m_1,n_1}\,F^{m_2,n_2}\,F^{m_3,n_3}}\right.\\ & \left. + \frac{F^{m_2,n_2}}{H^{m_2,n_2}\,F^{m_3,n_3}\,F^{m_1,n_1}} + \frac{F^{m_3,n_3}}{H^{m_3,n_3}\,F^{m_1,n_1}\,F^{m_2,n_2}}\right)\\ & + \hat\psi^{m_1,n_1}\,\hat\psi^{m_2,n_2}\,\hat\psi^{m_3,n_3}\left[\frac{2\,B_\theta\,B_\phi - r\,(\sigma/a)\,(B_\theta^2+B_\phi^2)}{F^{m_1,n_1}\,F^{m_2,n_2}\,F^{m_3,n_3}}\right]\Bigg\}.\end{aligned} \tag{136}$$

Let

$$X_\theta(r,t) = X_\theta^{m_1,n_1} + X_\theta^{m_2,n_2} + X_\theta^{m_3,n_3}, \tag{137}$$

$$X_\phi(r,t) = X_\phi^{m_1,n_1} + X_\phi^{m_2,n_2} + X_\phi^{m_3,n_3}. \tag{138}$$

According to Eqs. (122) and (124)

$$T_\theta(r,t) = \frac{\pi^2\,R_0}{\mu_0}\frac{\partial X_\theta}{\partial r}, \tag{139}$$

$$T_\phi(r,t) = -\frac{\pi^2\,R_0}{\mu_0}\frac{\partial X_\phi}{\partial r}. \tag{140}$$

However, it follows from Eqs. (130)–(135) that

$$\frac{\partial X_\theta}{\partial r} = \frac{\partial X_\phi}{\partial r} = 0, \tag{141}$$

where use has been made of Eqs. (21), (108), and (109). Hence, we deduce that zero flux-surface averaged electromagnetic torque is exerted throughout the bulk of the plasma as a consequence of the nonlinear coupling of tearing modes. This is the expected result because it is obvious from Eqs. (122) and (124) that zero flux-surface averaged electromagnetic torque can be exerted in any region of the plasma governed by the perturbed force balance equation, (12), given that $P+p$ is a single-valued function of θ and ϕ.

C. Localized electromagnetic torques

The previous demonstration that the nonlinear coupling of tearing modes gives rise to zero flux-surface averaged electromagnetic torque is valid in all regions of the plasma governed by Eq. (12). However, this equation breaks down in the immediate vicinity of the rational surfaces associated with the three coupled modes, so it is still possible that localized electromagnetic torques can develop at these surfaces. The fact that (the linearized form of) $(\psi^{m,n})'(r,t)$ is discontinuous (in r) across the (m,n) mode rational surface (see Sec. III B), whereas $\psi^{m,n}(r,t)$, the $\psi^{m',n'}(r,t)$, and the $(\psi^{m',n'})'(r,t)$ are continuous (where m', $n' \neq m, n$), implies from Eqs. (31)–(33), (123), and (125) that (to lowest order) $X_\theta^{m,n}(r,t)$ and $X_\phi^{m,n}(r,t)$ are also discontinuous across this surface, whereas the $X_\theta^{m',n'}(r,t)$ and $X_\phi^{m',n'}(r,t)$ are continuous. Thus, Eqs. (122) and (124) yield

$$T_\theta(r,t) = \sum_{m,n}\delta T_\theta(t)\,\delta(r - r_s^{m,n}), \tag{142}$$

$$T_\phi(r,t) = \sum_{m,n}\delta T_\phi(t)\,\delta(r - r_s^{m,n}), \tag{143}$$

where

$$\delta T_\theta^{m,n}(t) = \frac{\pi^2\,R_0}{\mu_0}\lim_{\delta\to 0}\left[X_\theta^{m,n}(r,t)\right]_{r=r_s^{m,n}-\delta}^{r=r_s^{m,n}+\delta}, \tag{144}$$

$$\delta T_\phi^{m,n}(t) = -\frac{\pi^2\,R_0}{\mu_0}\lim_{\delta\to 0}\left[X_\phi^{m,n}(r,t)\right]_{r=r_s^{m,n}-\delta}^{r=r_s^{m,n}+\delta}. \tag{145}$$

Here, it is understood that the delta functions appearing in Eqs. (142) and (143) represent radially thin regions, centered on each coupled rational surface, in which the perturbed force balance equation, Eq. (12), breaks down.

Now, the boundary conditions on the linearized tearing eigenfunctions discussed in Sec. III C suggest that $X_\theta^{m,n}(r,t)$ and $X_\phi^{m,n}(r,t)$ (which are constructed from the linear eigenfunctions) are zero at $r=0$ and $r=b$. Thus, Eq. (130) can be integrated to give

$$X_\theta^{m_1,n_1}(r,t) = \mathrm{Im}\left[(\Psi^{m_1,n_1}\,\Psi^{m_2,n_2})^*\,\Psi^{m_3,n_3}\right] \times\left[-m_1\int_0^r\tau(r')\,dr' + \frac{\sigma}{a}\frac{\hat\psi^{m_1,n_1}\,\hat\psi^{m_2,n_2}\,\hat\psi^{m_3,n_3}\,r\,B_\phi}{F^{m_2,n_2}\,F^{m_3,n_3}}\right], \tag{146}$$

for $0 \le r \le r_s^{m,n}$, and

$$X_\theta^{m_1,n_1}(r,t) = \mathrm{Im}\left[(\Psi^{m_1,n_1}\,\Psi^{m_2,n_2})^*\,\Psi^{m_3,n_3}\right] \times\left[m_1\int_r^b\tau(r')\,dr' + \frac{\sigma}{a}\frac{\hat\psi^{m_1,n_1}\,\hat\psi^{m_2,n_2}\,\hat\psi^{m_3,n_3}\,r\,B_\phi}{F^{m_2,n_2}\,F^{m_3,n_3}}\right], \tag{147}$$

for $r_s^{m,n} \le r \le b$. Clearly,[18]

$$\lim_{\delta\to 0}\left[X_\theta^{m_1,n_1}(r,t)\right]_{r=r_s^{m_1,n_1}-\delta}^{r=r_s^{m_1,n_1}+\delta} = \mathrm{Im}\left[(\Psi^{m_1,n_1}\,\Psi^{m_2,n_2})^*\,\Psi^{m_3,n_3}\right] m_1\int_0^a\tau(r)\,dr. \tag{148}$$

Note that we can change the upper limit of integration of the integral in the previous expression from b to a, because $\tau(r) = 0$ in the vacuum region surrounding the plasma (where $\sigma' = 0$). Similarly, integration of Eqs. (131)–(135) yields

$$\lim_{\delta\to 0}\left[X_\theta^{m_2,n_2}(r,t)\right]_{r=r_s^{m_2,n_2}-\delta}^{r=r_s^{m_2,n_2}+\delta} = \mathrm{Im}\left[(\Psi^{m_1,n_1}\,\Psi^{m_2,n_2})^*\,\Psi^{m_3,n_3}\right] m_2\int_0^a\tau(r)\,dr, \tag{149}$$

23 April 2024 14:39:08

© Author(s) 2024

$$\lim_{\delta\to 0}\left[X_\theta^{m_3,n_3}(r,t)\right]_{r=r_s^{m_3,n_3}-\delta}^{r=r_s^{m_3,n_3}+\delta} = -\mathrm{Im}\left[(\Psi^{m_1,n_1}\,\Psi^{m_2,n_2})^*\,\Psi^{m_3,n_3}\right] m_3 \int_0^a \tau(r)\,dr, \tag{150}$$

$$\lim_{\delta\to 0}\left[X_\phi^{m_1,n_1}(r,t)\right]_{r=r_s^{m_1,n_1}-\delta}^{r=r_s^{m_1,n_1}+\delta} = \mathrm{Im}\left[(\Psi^{m_1,n_1}\,\Psi^{m_2,n_2})^*\,\Psi^{m_3,n_3}\right] n_1 \int_0^a \tau(r)\,dr, \tag{151}$$

$$\lim_{\delta\to 0}\left[X_\phi^{m_2,n_2}(r,t)\right]_{r=r_s^{m_2,n_2}-\delta}^{r=r_s^{m_2,n_2}+\delta} = \mathrm{Im}\left[(\Psi^{m_1,n_1}\,\Psi^{m_2,n_2})^*\,\Psi^{m_3,n_3}\right] n_2 \int_0^a \tau(r)\,dr, \tag{152}$$

$$\lim_{\delta\to 0}\left[X_\phi^{m_3,n_3}(r,t)\right]_{r=r_s^{m_3,n_3}-\delta}^{r=r_s^{m_3,n_3}+\delta} = -\mathrm{Im}\left[(\Psi^{m_1,n_1}\,\Psi^{m_2,n_2})^*\,\Psi^{m_3,n_3}\right] n_3 \int_0^a \tau(r)\,dr. \tag{153}$$

The previous analysis suggests that[18]

$$\delta T_\theta^{m_1,n_1}(t) = \frac{\pi^2 R_0}{\mu_0}\,\mathrm{Im}\left[(\Psi^{m_1,n_1}\,\Psi^{m_2,n_2})^*\,\Psi^{m_3,n_3}\right] m_1 J^{m_1,n_1;m_2,n_2;m_3,n_3}(a), \tag{154}$$

$$\delta T_\theta^{m_2,n_2}(t) = \frac{\pi^2 R_0}{\mu_0}\,\mathrm{Im}\left[(\Psi^{m_1,n_1}\,\Psi^{m_2,n_2})^*\,\Psi^{m_3,n_3}\right] m_2 J^{m_1,n_1;m_2,n_2;m_3,n_3}(a), \tag{155}$$

$$\delta T_\theta^{m_3,n_3}(t) = -\frac{\pi^2 R_0}{\mu_0}\,\mathrm{Im}\left[(\Psi^{m_1,n_1}\,\Psi^{m_2,n_2})^*\,\Psi^{m_3,n_3}\right] m_3 J^{m_1,n_1;m_2,n_2;m_3,n_3}(a), \tag{156}$$

and

$$\delta T_\phi^{m_1,n_1}(t) = -\frac{\pi^2 R_0}{\mu_0}\,\mathrm{Im}\left[(\Psi^{m_1,n_1}\,\Psi^{m_2,n_2})^*\,\Psi^{m_3,n_3}\right] n_1 J^{m_1,n_1;m_2,n_2;m_3,n_3}(a), \tag{157}$$

$$\delta T_\phi^{m_2,n_2}(t) = -\frac{\pi^2 R_0}{\mu_0}\,\mathrm{Im}\left[(\Psi^{m_1,n_1}\,\Psi^{m_2,n_2})^*\,\Psi^{m_3,n_3}\right] n_2 J^{m_1,n_1;m_2,n_2;m_3,n_3}(a), \tag{158}$$

$$\delta T_\phi^{m_3,n_3}(t) = \frac{\pi^2 R_0}{\mu_0}\,\mathrm{Im}\left[(\Psi^{m_1,n_1}\,\Psi^{m_2,n_2})^*\,\Psi^{m_3,n_3}\right] n_3 J^{m_1,n_1;m_2,n_2;m_3,n_3}(a), \tag{159}$$

where

$$J^{m_1,n_1;m_2,n_2;m_3,n_3}(r) = \int_0^r \tau(r')\,dr' \tag{160}$$

is termed the *overlap integral*. Note, incidentally, that the expressions for the nonlinear torques given in Ref. 18 erroneously differ from the expressions (154)–(159) by a factor of 2.

According to Eqs. (108), (109), and (154)–(159),

$$\delta T_\theta^{m_1,n_1}(t) + \delta T_\theta^{m_2,n_2}(t) + \delta T_\theta^{m_3,n_3}(t) = 0, \tag{161}$$

$$\delta T_\phi^{m_1,n_1}(t) + \delta T_\phi^{m_2,n_2}(t) + \delta T_\phi^{m_3,n_3}(t) = 0. \tag{162}$$

In other words, the sum of all of the localized nonlinear electromagnetic torques acting within the plasma is zero, as is required by the conservation of angular momentum.

D. Nonlinear tearing mode dispersion relation

Consider the nonlinear coupling of the (m_1, n_1), the (m_2, n_2), and the (m_3, n_3) tearing modes, where the poloidal and toroidal mode numbers are related according to Eqs. (108) and (109), respectively. Asymptotic matching across the three coupled rational surfaces yields the nonlinear dispersion relations of the three modes,

$$\Delta\Psi^{m_1,n_1}(t) = \Delta^{m_1,n_1}\,\Psi^{m_1,n_1}(t) + \Xi^{m_1,n_1}(t), \tag{163}$$

$$\Delta\Psi^{m_2,n_2}(t) = \Delta^{m_2,n_2}\,\Psi^{m_2,n_2}(t) + \Xi^{m_2,n_2}(t), \tag{164}$$

$$\Delta\Psi^{m_3,n_3}(t) = \Delta^{m_3,n_3}\,\Psi^{m_3,n_3}(t) + \Xi^{m_3,n_3}(t), \tag{165}$$

where Ξ^{m_1,n_1}, Ξ^{m_2,n_2}, and Ξ^{m_3,n_3} are the nonlinear corrections. Here, use has been made of Eqs. (72), (75)–(77), and (107). However, it follows from Eqs. (31)–(33), (72), (75), (76), (123), (125), (144), and (145) that, to lowest order,

$$\delta T_\theta^{m,n}(t) = -\frac{2\pi^2 R_0}{\mu_0}\,m\,\mathrm{Im}\left[\Delta\Psi^{m,n}\,(\Psi^{m,n})^*\right], \tag{166}$$

$$\delta T_\phi^{m,n}(t) = \frac{2\pi^2 R_0}{\mu_0}\,n\,\mathrm{Im}\left[\Delta\Psi^{m,n}\,(\Psi^{m,n})^*\right]. \tag{167}$$

A comparison between Eqs. (154)–(159) and the previous two equations reveals that[18]

$$\Xi^{m_1,n_1}(t) = -\frac{1}{2}\,(\Psi^{m_2,n_2})^*\,\Psi^{m_3,n_3}\,J^{m_1,n_1;m_2,n_2;m_3,n_3}(a), \tag{168}$$

$$\Xi^{m_2,n_2}(t) = -\frac{1}{2}\,(\Psi^{m_1,n_1})^*\,\Psi^{m_3,n_3}\,J^{m_1,n_1;m_2,n_2;m_3,n_3}(a), \tag{169}$$

$$\Xi^{m_3,n_3}(t) = -\frac{1}{2}\,\Psi^{m_1,n_1}\,\Psi^{m_2,n_2}\,J^{m_1,n_1;m_2,n_2;m_3,n_3}(a). \tag{170}$$

E. Regularization at rational surfaces

The linearized (m, n) perturbed magnetic field, $\mathbf{b}_L^{m,n}(\mathbf{r},t)$, is related to the ideal (m, n) plasma displacement, $\boldsymbol{\xi}^{m,n}(\mathbf{r},t)$, via[4]

$$\mathbf{b}_L^{m,n} = \nabla\times(\boldsymbol{\xi}^{m,n}\times\mathbf{B}). \tag{171}$$

It follows that

$$\mathbf{b}_L^{m,n} = (\mathbf{B}\cdot\nabla)\,\boldsymbol{\xi}^{m,n} - (\boldsymbol{\xi}^{m,n}\cdot\nabla)\,\mathbf{B}, \tag{172}$$

given that $\nabla\cdot\mathbf{b}_L^{m,n} = 0$, and assuming that $\nabla\cdot\boldsymbol{\xi}^{m,n} = 0$.[4] Making use of Eqs. (19), (21), (82), and (88), we obtain

$$\xi_r^{m,n}(r,t) = \Psi^{m,n}(t)\,\frac{\hat{\psi}^{m,n}(r)}{F^{m,n}(r)}. \tag{173}$$

In the immediate vicinity of the (m, n) rational surface, the previous expression reduces to

$$\xi_r^{m,n} \simeq \frac{\Psi^{m,n}}{r_s^{m,n}\,(F^{m,n})'_{r=r_s^{m,n}}\,x}, \tag{174}$$

where x is specified in Eq. (73). According to the previous equation, the radial displacement of magnetic flux-surfaces associated with an

23 April 2024 14:39:08

© Author(s) 2024

(m, n) tearing mode is singular at the (m, n) rational surface ($x = 0$). In reality, the magnitude of the displacement is limited by the change in topology of magnetic flux-surfaces consequent on the formation of a magnetic island chain at the rational surface.[6] The full radial width of the magnetic island chain that forms at the (m, n) rational surface is[28]

$$W^{m,n}(t) = 4\,|\Psi^{m,n}|^{1/2}\left[\frac{(H^{mn})^{1/2}}{|(F^{m,n})'|}\right]^{1/2}_{r=r_s^{m,n}}. \tag{175}$$

The plasma displacement attains its maximum value at the edge of the island chain (i.e., when $|x| \sim W^{m,n}/r_s^{m,n}$). It follows that the peak value of $|\hat{\psi}^{m,n}/F^{m,n}|$ in the vicinity of the (m, n) rational surface is

$$\left|\frac{\hat{\psi}^{m,n}}{F^{m,n}}\right|_{\max} \simeq \frac{1}{|(F^{m,n})'|_{r=r_s^{m\,n}}\,W^{m,n}} = \left(\frac{q}{\epsilon\,B_\phi}\right)_{r=r_s^{m\,n}} \frac{1}{n\,|q'|_{r=r_s^{m\,n}}\,W^{m,n}}. \tag{176}$$

Note that the function $\tau(r)$, defined in Eq. (136), is singular at the three coupled rational surfaces. However, a comparison with Eq. (173) reveals that these singularities are associated with the singularities of the resonant harmonics of the ideal plasma displacements at the rational surfaces. Because, in reality, the ideal displacements are not actually singular at the rational surfaces, it follows that the function $\tau(r)$ is also not singular at the rational surfaces. Thus, when evaluating the overlap integral, $\int_0^a \tau(r)\,dr$, we can regularize the function $\tau(r)$ by writing

$$\frac{1}{F^{m,n}} \to \frac{q}{\epsilon\,B_\phi}\,\frac{m - n\,q}{(m - n\,q)^2 + \left[(n\,q')_{r=r_s^{m\,n}}\,W^{m,n}\right]^2}. \tag{177}$$

Similarly,

$$\frac{1}{m - n\,q} \to \frac{m - n\,q}{(m - n\,q)^2 + \left[(n\,q')_{r=r_s^{m\,n}}\,W^{m,n}\right]^2}, \tag{178}$$

in Eq. (68).

F. Validity of quasilinear approach

Constructing the nonlinear coupling coefficients, $\mathbf{A}^{m,n}$, from the linear eigenfunctions is only accurate if the nonlinear contributions to the expressions for (say) $b_\theta^{m_3,n_3}$ and $b_\phi^{m_3,n_3}$, given in Eqs. (32) and (33), are smaller than the linear contributions. The linear contributions are the first two terms on the right-hand sides of the equations, whereas the nonlinear contributions are the final terms involving $A_r^{m_3,n_3}$. Roughly speaking, in the general case, the condition for the nonlinear terms to be smaller than the linear terms is

$$\left(\frac{W^{m_3,n_3}}{a}\right)^2 \gg \left(\frac{W^{m_1,n_1}}{a}\right)^2\left(\frac{W^{m_2,n_2}}{a}\right)^2. \tag{179}$$

Making use of the regularization procedure discussed in Sec. IV E, in the immediate vicinity of the (m_1, n_1) rational surface the condition becomes

$$\left(\frac{W^{m_3,n_3}}{a}\right)^2 \gg \left(\frac{W^{m_1,n_1}}{a}\right)\left(\frac{W^{m_2,n_2}}{a}\right)^2. \tag{180}$$

Likewise, in the immediate vicinity of the (m_2, n_2) rational surface the condition becomes

$$\left(\frac{W^{m_3,n_3}}{a}\right)^2 \gg \left(\frac{W^{m_1,n_1}}{a}\right)^2\left(\frac{W^{m_2,n_2}}{a}\right). \tag{181}$$

Thus, the condition is satisfied in all cases provided that

$$\frac{W^{m_1,n_1}}{a}, \frac{W^{m_2,n_2}}{a}, \frac{W^{m_2,n_2}}{a} \ll 1. \tag{182}$$

In other words, the condition is satisfied provided that the radial widths of the magnetic island chains in the plasma are all much less than the plasma minor radius.

V. SLINKY PATTERN FORMATION IN RFP PLASMAS

A. Introduction

A reversed field pinch is characterized by a safety-factor profile that is everywhere much less than unity and decreases with increasing plasma minor radius,[2,3] see Fig. 1. The safety-factor passes through zero in the outer regions of the plasma at the so-called *reversal surface*, where the equilibrium toroidal magnetic field changes direction. The plasma is unstable to multiple $m = 1$ tearing modes, resonant at different rational surfaces in the plasma core (i.e., inside the reversal surface), and also to multiple $m = 0$ tearing modes that are all resonant at the reversal surface.[9] The various unstable $m = 1$ and $m = 0$ modes invariably phase lock to one another to produce a characteristic toroidally localized pattern in the perturbed magnetic field that is known as the slinky pattern.[11–13]

B. Phase locking of $m = 0$ modes

Making use of Eqs. (19), (37), (38), (77), (79), (82)–(84), (88)–(90), and (107), as well as the fact that $\hat{\psi}^{m,n}(r)$ is continuous across a rational surface (see Sec. III B), whereas $d\hat{\psi}^{m,n}/dr$ is discontinuous, the linear resonant component of the radial magnetic field at the (m, n) rational surface is

$$b_r(\theta, \phi) = -\frac{B_0}{\hat{r}_s^{m,n}}\,\hat{\Psi}^{m,n}\,\sin(m\,\theta - n\,\phi + \varphi^{m,n}), \tag{183}$$

whereas the poloidal and toroidal components of the radially integrated helical current sheet that flows at the surface are

$$K_\theta(\theta, \phi) = -\frac{B_0}{\mu_0}\left(\frac{n\,\epsilon}{\hat{r}\,H^{m,n}}\right)_{r_s^{m,n}} \hat{\Psi}^{m,n}\,\Delta^{m,n}\,\cos(m\,\theta - n\,\phi + \varphi^{m,n}), \tag{184}$$

$$K_\phi(\theta, \phi) = -\frac{B_0}{\mu_0}\left(\frac{m}{\hat{r}\,H^{m,n}}\right)_{r_s^{m,n}} \hat{\Psi}^{m,n}\,\Delta^{m,n}\,\cos(m\,\theta - n\,\phi + \varphi^{m,n}), \tag{185}$$

respectively. Here, $\hat{r} = r/a$ and $\hat{r}_s^{m,n} = r_s^{m,n}/a$. Moreover, we have written

$$\Psi^{m,n}(t) = a\,B_0\,\hat{\Psi}^{m,n}(t)\,e^{i\varphi^{m,n}(t)}, \tag{186}$$

where $B_0 = B_\phi(0)$, $\hat{\Psi}^{m,n}(t)$ is real, positive, and dimensionless, and $\varphi^{m,n}(t)$ is a helical phase angle. The lowest-order non-flux-surface-averaged poloidal and toroidal electromagnetic torques that are exerted on the plasma in the vicinity of the (m, n) rational surface are

23 April 2024 14:39:08

© Author(s) 2024

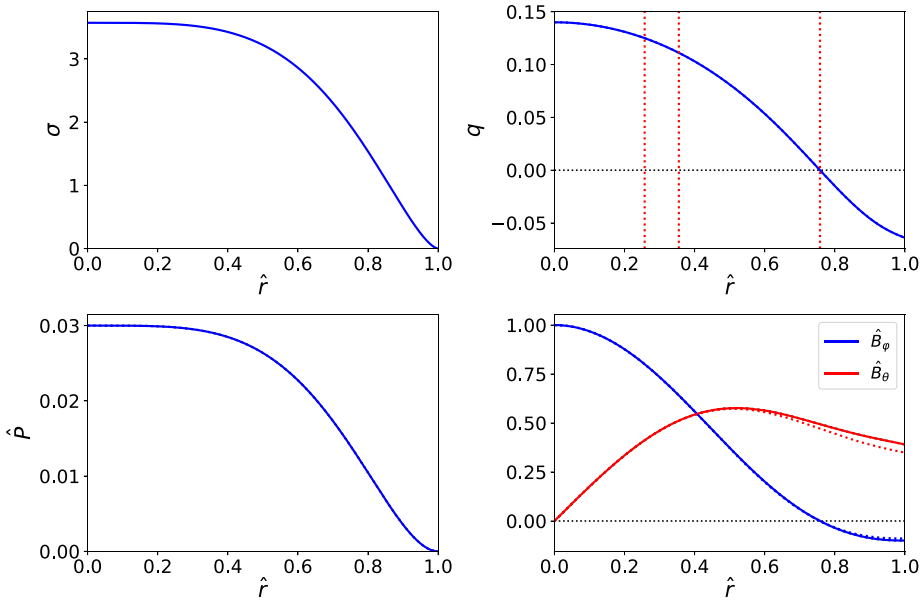

FIG. 1. Stepped pressure RFP equilibrium characterized by $\epsilon_a = 0.25$, $q_0 = 0.14$, $\beta_0 = 0.06$, $\alpha_\sigma = 4$, $\nu_\sigma = 1.6$, $\alpha_p = 4$, and $\nu_p = 2$. There are 500 equally spaced control surfaces in the plasma. Here, σ is the (normalized) parallel current profile, q the safety-factor profile, $\hat{P}$ the (normalized) pressure profile, $\hat{B}_\theta$ the (normalized) poloidal magnetic field profile, and $\hat{B}_\phi$ the (normalized) toroidal magnetic field profile. The vertical lines in the safety-factor plot indicate the locations of the (1, 8), (1, 9), and (0, 1) rational surfaces, in order from the left to the right. The dotted curves in the magnetic field plot show the zero pressure magnetic field profiles. Here, $\hat{r}$ represents normalized radial distance from the magnetic axis.

$$\delta T_\theta(\theta,\phi) = R_0\,(r_s^{m,n})^2\,b_r(\theta,\phi)\,K_\phi(\theta,\phi), \tag{187}$$

$$\delta T_\phi(\theta,\phi) = -R_0^2\,r_s^{m,n}\,b_r(\theta,\phi)\,K_\theta(\theta,\phi), \tag{188}$$

respectively [see Eqs. (122) and (124)]. It follows that

$$\delta T_\theta(\theta,\phi) = \frac{B_0^2\,R_0\,a^2}{\mu_0}\,\frac{m}{2\,H^{m,n}(r_s^{m,n})}\,(\hat{\Psi}^{m,n})^2\,\Delta^{m,n} \times \sin[2(m\,\theta - n\,\phi + \varphi^{m,n})], \tag{189}$$

$$\delta T_\phi(\theta,\phi) = -\frac{B_0^2\,R_0\,a^2}{\mu_0}\,\frac{n}{2\,H^{m,n}(r_s^{m,n})}\,(\hat{\Psi}^{m,n})^2\,\Delta^{m,n} \times \sin[2(m\,\theta - n\,\phi + \varphi^{m,n})]. \tag{190}$$

Note that $\delta T_\theta(\theta,\phi)$ and $\delta T_\phi(\theta,\phi)$ both average to zero around the rational flux-surface. This behavior is what allows the higher order (because they scale as the cube, rather than the square, of the mode amplitude) nonlinear torques (154)–(159) to play a significant role in tearing mode dynamics.

The previous analysis applies to the unstable $m = 1$ modes, which are resonant at different rational surfaces in the plasma. However, the unstable $m = 0$ modes are all resonant at the reversal surface, whose radius is (say) r_v. Thus, the resonant component of the radial magnetic field at the reversal surface is

$$b_r^{m=0}(\phi) = \frac{B_0}{\hat{r}_v}\sum_n \hat{\Psi}^{0,n}\,\sin\left(n\,\phi - \varphi^{0,n}\right), \tag{191}$$

where the sum is over the toroidal mode numbers of the unstable $m = 0$ modes, and $\hat{r}_v = r_v/a$. Likewise, the radially integrated poloidal current sheet that flows at the reversal surface is

$$K_\theta^{m=0}(\phi) = -\frac{B_0\,R_0}{\mu_0\,a\,\hat{r}_v^2}\sum_n \frac{\hat{\Psi}^{0,n}}{n}\,\Delta^{0,n}\,\cos\left(n\,\phi - \varphi^{0,n}\right). \tag{192}$$

Thus, the lowest-order non-flux-surface-averaged toroidal electromagnetic torque that is exerted on the plasma at the reversal surface is

$$\delta T_\phi(\phi) = \frac{B_0^2\,R_0\,a^2}{\mu_0}\left(\frac{R_0}{r_v}\right)^2\sum_{n,n'}\frac{\hat{\Psi}^{0,n}\,\hat{\Psi}^{0,n'}\,\Delta^{0,n'}}{n'} \times \sin\left(n\,\phi - \varphi^{0,n}\right)\cos\left(n'\,\phi - \varphi^{0,n'}\right). \tag{193}$$

Note that this torque averages to zero around the reversal flux-surface. Nevertheless, the amplitude of the torque is larger than the torques (189) and (190) by a factor $(R_0/r_v)^2$ (assuming similar $m = 0$ and $m = 1$ mode amplitudes), which is a substantial factor in a conventional RFP. Following Ref. 19, we hypothesize that the large torque exerted at the reversal surface drives local plasma flows that rearrange the helical phases of the various $m = 0$ modes in such a manner as to *minimize* the amplitude of the torque.

Let us assume that the $m = 0$ modes phase lock-in such a manner that

$$\varphi^{0,n} = n\,\phi_0 - \Delta_0. \tag{194}$$

This assumed phase relation can be justified via a variational argument.[19] It follows that

$$\delta T_\phi(\phi) = \frac{B_0^2\,R_0\,a^2}{\mu_0}\left(\frac{R_0}{r_v}\right)^2\delta\hat{T}_\phi(\phi), \tag{195}$$

where

$$\delta\hat{T}_\phi(\phi) = \sum_{k>0}(C_k\,\cos[k\,(\phi-\phi_0)] + S_k\,\sin[k\,(\phi-\phi_0)]), \tag{196}$$

and

$$C_k = a_k\,\sin(2\,\Delta_0), \tag{197}$$

$$S_k = a_k\,\cos(2\,\Delta_0) + b_k, \tag{198}$$

$$a_k = \frac{1}{2}\sum_n \frac{\hat{\Psi}^{0,n}\,\hat{\Psi}^{0,k-n}\,\Delta^{0,n}}{n}, \tag{199}$$

23 April 2024 14:39:08

© Author(s) 2024

$$b_k = \frac{1}{2}\sum_n \hat{\Psi}^{0,n}\,\hat{\Psi}^{0,n+k}\left(\frac{\Delta^{0,n}}{n} - \frac{\Delta^{0,n+k}}{n+k}\right). \tag{200}$$

Now, the mean square of the normalized toroidal torque exerted at the reversal surface is

$$\oint \left[\delta\hat{T}_\phi(\phi)\right]^2 \frac{d\phi}{2\pi} = \frac{1}{2}\sum_{k>0}\left(C_k^2 + S_k^2\right) = \frac{1}{2}\sum_{k>0}\left[a_k^2 + 2\,a_k\,b_k\,\cos(2\,\Delta_0) + b_k^2\right]. \tag{201}$$

Note that the a_k are all positive definite. Moreover, as long as $\Delta^{0,n}$ is a decreasing function of increasing n, as is generally the case (see Fig. 3), we deduce that the b_k are all positive. Thus, the mean square torque assumes its minimum value,

$$\oint \left[\delta\hat{T}_\phi(\phi)\right]^2 \frac{d\phi}{2\pi} = \frac{1}{2}\sum_{k>0}(a_k - b_k)^2, \tag{202}$$

when $\cos(2\,\Delta_0) = -1$. Hence, we conclude that the unstable $m=0$ tearing modes in the plasma phase lock-in such a manner that $\Delta_0 = \pm\pi/2$.[19]

Making use of Eqs. (191) and (194), the $m=0$ radial magnetic field at the reversal surface is

$$b_r^{m=0}(\phi) = B_0\,\frac{\sin\Delta_0}{\hat{r}_v}\sum_n \hat{\Psi}^{0,n}\,\cos[n\,(\phi-\phi_0)]. \tag{203}$$

It can be seen that the $m=0$ modes phase lock such that their radial fields interfere constructively at $\phi=\phi_0$. Consequently, there is a toroidally localized spike in the $m=0$ radial magnetic field at $\phi=\phi_0$ (see Fig. 4).

Note that ϕ_0 is undetermined. In fact, if we adopt the simplistic assumption that $m=0$ modes are convected by the plasma at the reversal surface,[40] then we conclude that

$$\frac{d\phi_0}{dt} = \Omega_\phi(r_v), \tag{204}$$

where $\Omega_\phi(r)$ is the equilibrium plasma toroidal angular velocity profile. It follows that the toroidally localized spike in the $m=0$ radial magnetic field is convected by the plasma at the reversal surface. However, the spike may lock to gaps in the conducting wall surrounding the plasma.[19,26,41] in which case ϕ_0 becomes constant in time, and the toroidal plasma rotation at the reversal surface is arrested.

C. Phase locking of $m=1$ modes

According to Eqs. (158) and (186), the flux-surface integrated, nonlinear, toroidal electromagnetic torque exerted at the reversal surface as a consequence of the coupling of the $(1,n)$, $(0,k)$, and $(1,n+k)$ tearing modes is

$$T_\phi^{n,k} = -\frac{\pi^2\,B_0^2\,R_0\,a^2}{\mu_0}\,\hat{\Psi}^{1,n}\,\hat{\Psi}^{0,k}\,\hat{\Psi}^{1,n+k}\,\hat{\jmath}^{n,k}\,k\,\sin\left(\varphi^{1,n+k} - \varphi^{1,n} - \varphi^{0,k}\right), \tag{205}$$

where

$$\hat{\jmath}^{n,k} = B_0\,a\,J^{1,n;0,k;1,n+k}(a) \tag{206}$$

is a dimensionless measure of the coupling strength. Thus, the total nonlinear torque exerted at the reversal surface can be written

$$T_\phi = \frac{\pi^2\,B_0^2\,R_0\,a^2}{\mu_0}\,\hat{T}_\phi, \tag{207}$$

where

$$\hat{T}_\phi = -\sum_{n,k}\hat{\Psi}^{1,n}\,\hat{\Psi}^{0,k}\,\hat{\Psi}^{1,n+k}\,\hat{\jmath}^{n,k}\,k\,\sin\left(\varphi^{1,n+k} - \varphi^{1,n} - \varphi^{0,k}\right). \tag{208}$$

Here, the sum is over the toroidal mode numbers of all the unstable $m=1$ and $m=0$ modes. Again following Ref. 19, we hypothesize that the nonlinear torque exerted at the reversal surface, and the associated torques exerted at the $m=1$ rational surfaces, drive flows in the plasma core that rearrange the helical phases of the various $m=1$ modes so as to *minimize* the torque. Note that this hypothesis was verified by plasma dynamic simulations described in Ref. 19.

Let us assume that the $m=1$ modes phase lock such that

$$\varphi^{1,n} = n\,\phi_1 - \Delta_1. \tag{209}$$

Making use of Eq. (194), as well as the fact that $\Delta_0 = \pm\pi/2$, it follows that

$$\hat{T}_\phi(\phi_1-\phi_0) = -\sin(\Delta_0)\sum_{n,k}\hat{\Psi}^{1,n}\,\hat{\Psi}^{0,k}\,\hat{\Psi}^{1,n+k}\,\hat{\jmath}^{n,k}\,k \times \cos[k\,(\phi_1-\phi_0)]. \tag{210}$$

If we write

$$\hat{T}(\phi) = \frac{dV}{d\phi}, \tag{211}$$

then the so-called *locking potential* takes the form

$$V(\phi_1-\phi_0) = -\sin(\Delta_0)\sum_{n,k}\hat{\Psi}^{1,n}\,\hat{\Psi}^{0,k}\,\hat{\Psi}^{1,n+k}\,\hat{\jmath}^{n,k}\,\sin[k\,(\phi_1-\phi_0)]. \tag{212}$$

The torque (210) is set to zero at a minimum of the locking potential (a maximum of the potential is dynamically unstable). In other words, $\phi_1-\phi_0$ takes a fixed value that is determined by finding the minimum of the locking potential (see Fig. 8).

The net $m=1$ radial magnetic field at the reversal surface due to the $m=1$ modes resonant in the plasma core can be written

$$b_r^{m=1}(\theta,\phi) = B_0\,C^{m=1}(\phi-\phi_1)\,\cos(\theta-\Delta_1) + B_0\,S^{m=1}(\phi-\phi_1)\,\sin(\theta-\Delta_1), \tag{213}$$

where

$$C^{m=1}(\phi-\phi_1) = \sum_n \frac{\hat{\Psi}^{1,n}\,\hat{\psi}^{1,n}(r_v)}{\hat{r}_v}\,\sin[n\,(\phi-\phi_1)], \tag{214}$$

$$S^{m=1}(\phi-\phi_1) = -\sum_n \frac{\hat{\Psi}^{1,n}\,\hat{\psi}^{1,n}(r_v)}{\hat{r}_v}\,\cos[n\,(\phi-\phi_1)]. \tag{215}$$

It is clear that the radial fields of the phase-locked $m=1$ modes interfere constructively at $\phi=\phi_1$ (see Fig. 7). Moreover, ϕ_1 is tied to ϕ_0.

23 April 2024 14:39:08

© Author(s) 2024

Thus, we deduce that the unstable $m = 1$ and $m = 0$ tearing modes in the plasma generate toroidally localized perturbations in the radial magnetic field that are phase locked to one another, and that co-rotate with the plasma at the reversal surface. These phase-locked perturbations constitute the slinky pattern. Note that Δ_1 is undetermined. In fact, this parameter generally increases linearly in time at a rate determined by flows in the plasma core.[19]

VI. EXAMPLE CALCULATION

A. Plasma equilibrium

It is helpful to define the dimensionless quantities $\hat{r} = r/a$, $\hat{b} = b/a$, $\hat{r}_i = r_i/a$, $\hat{W}^{m,n} = W^{m,n}/a$, $\hat{B}_\theta = B_\theta/B_0$, $\hat{B}_\phi = B_\phi/B_0$, $\hat{b}_r^{m=0} = b_r^{m=0}/B_0$, $\hat{P}(\hat{r}) = \mu_0 P(r)/B_0^2$, $\hat{\tau}(\hat{r}) = a^2 B_0 \tau(r)$, where $B_0 = B_\phi(0)$.

Our model parallel current and continuous pressure profiles are

$$\sigma(\hat{r}) = \frac{2\,\epsilon_a}{q_0}(1 - \hat{r}^{\alpha_\sigma})^{\nu_\sigma}, \tag{216}$$

$$\hat{P}_{\text{continuous}}(\hat{r}) = \frac{\beta_0}{2}(1 - \hat{r}^{\alpha_p})^{\nu_p}, \tag{217}$$

respectively. In the stepped pressure equilibrium, the pressures between the control surfaces are $\hat{P}_{\text{stepped}}(\hat{r}) = \hat{P}_i$ for $\hat{r}_i < \hat{r} < \hat{r}_{i+1}$, where $\hat{P}_i = \hat{P}_{\text{continuous}}(\hat{r}_i)$ (see Sec. III A).

Figure 1 shows a stepped pressure RFP equilibrium characterized by $\epsilon_a = 0.25$, $q_0 = 0.14$, $\beta_0 = 0.06$, $\alpha_\sigma = 4$, $\nu_\sigma = 1.6$, $\alpha_p = 4$, and $\nu_p = 2$. The corresponding zero pressure equilibrium magnetic fields are also shown. There are 500 equally spaced control surfaces in the plasma. With this many control surfaces, the stepped pressure equilibrium is essentially indistinguishable from the continuous equilibrium obtained by integrating Eqs. (8) and (9), using the continuous profiles (216) and (217). The equilibrium has all of the expected features of a RFP equilibrium. Namely, it possesses a fairly broad parallel current profile, a safety-factor profile that is much less than unity and decreases with increasing minor radius, and a toroidal magnetic field that reverses direction in the outer regions of the plasma. It is clear from the figure that the equilibrium pressure gradient leads to a modest increase in the poloidal magnetic field in the outer regions of the plasma, as well as a slight strengthening of the reversal of the toroidal magnetic field.

It is conventional to parameterize an RFP equilibrium in terms of the *pinch parameter*, $\Theta = B_\theta(a)/\langle B_\phi \rangle$, and the *reversal parameter*, $F = B_\phi(a)/\langle B_\phi \rangle$, where $\langle \cdots \rangle$ denotes a volume average.[2,3] The pinch and reversal parameters for the zero pressure equilibrium (i.e., $\beta_0 = 0$) shown in Fig. 1 are 1.88 and −0.48, respectively, whereas the corresponding quantities for the finite pressure equilibrium (i.e., $\beta_0 = 0.06$) are 2.12 and −0.54.

B. Tearing eigenfunctions

Figure 2 shows the linear eigenfunctions of the tearing mode triplet $(1, 8) + (0, 1) = (1, 9)$ calculated from the stepped pressure equilibrium shown in Fig. 1. The zero pressure eigenfunctions are also shown. The normalized radius of the perfectly conducting wall surrounding the plasma is $\hat{b} = 1.01$. Note that there are a sufficient number of control surfaces in the plasma that the eigenfunctions, and their radial derivatives, appear completely smooth. It can be seen that the equilibrium pressure gradient significantly modifies the eigenfunctions in the region outside the corresponding rational surfaces.

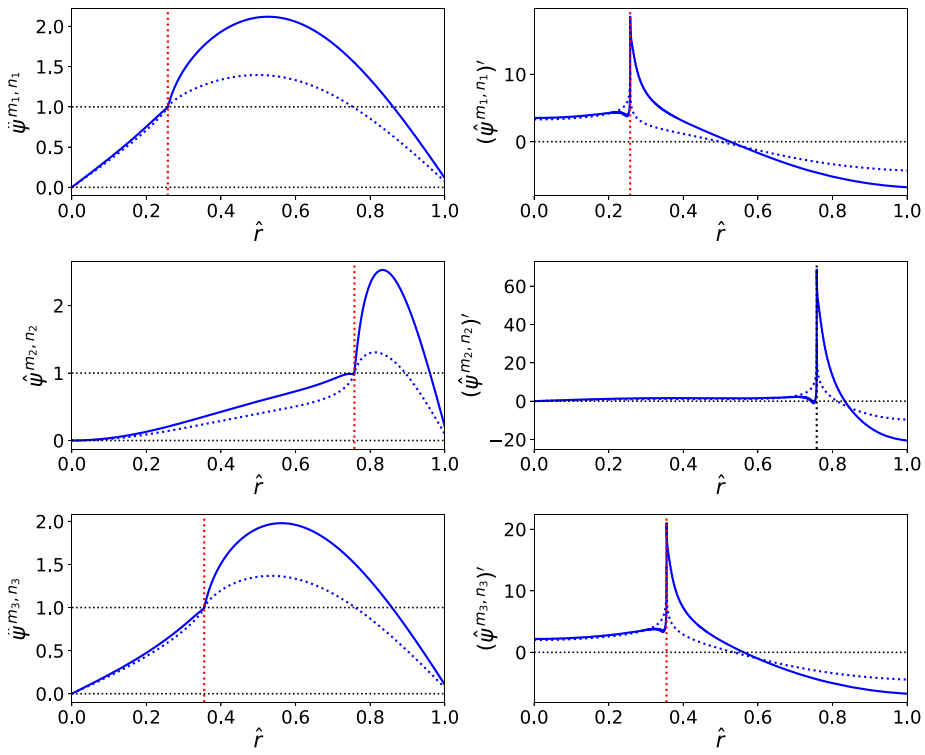

FIG. 2. Normalized tearing eigenfunctions, and their radial derivatives, for the stepped pressure equilibrium shown in Fig. 1. Here, $(m_1, n_1) = (1, 8)$, $(m_2, n_2) = (0, 1)$, and $(m_3, n_3) = (1, 9)$. The wall radius is $\hat{b} = 1.01$. The vertical lines indicate the locations of the rational surfaces. The dotted curves show the zero pressure eigenfunctions. Here, $\hat{r}$ represents normalized radial distance from the magnetic axis.

23 April 2024 14:39:08

© Author(s) 2024

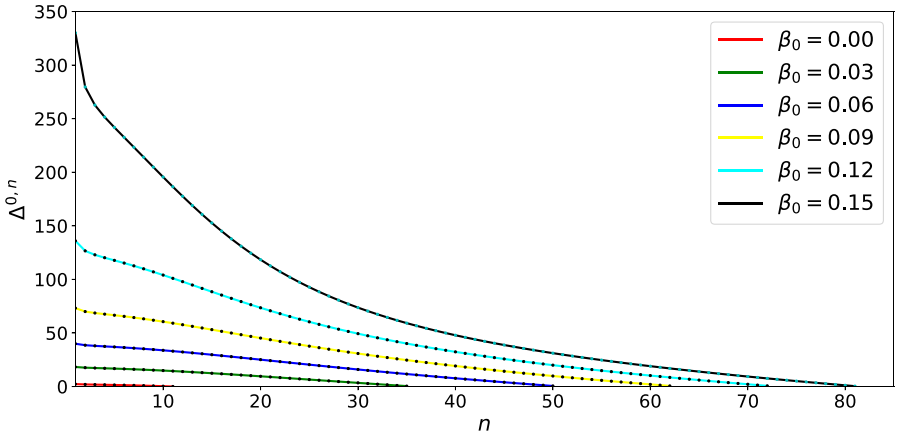

FIG. 3. Tearing stability indices of unstable $m = 0$ modes in a stepped pressure RFP equilibrium characterized by $\epsilon_a = 0.25$, $q_0 = 0.14$, $\alpha_\sigma = 4$, $\nu_\sigma = 1.6$, $\alpha_p = 4$, $\nu_p = 2$, $\hat{b} = 1.01$, and various different values of β_0. There are 500 equally spaced control surfaces in the plasma. Here, n is the toroidal mode number.

C. $m = 0$ modes

Figure 3 shows the tearing stability indices of the unstable $m = 0$ modes in our example RFP equilibrium, calculated as functions of the normalized equilibrium plasma pressure, β_0. It can be seen that at zero pressure, there are 11 unstable $m = 0$ tearing modes. Moreover, as the pressure is increased, more and more modes become unstable. In all cases, the tearing stability index, $\Delta^{0,n}$, is a decreasing function of increasing toroidal mode number, n. The (0, 1) mode actually becomes ideally unstable at $\beta_0 = 0.176$. Hence, this is the effective beta limit for the equilibrium.[4] As expected, the beta limit decreases as the perfectly conducting wall surrounding the plasma becomes more distant from the plasma (i.e., as $\hat{b}$ increases).

Figure 4 shows the phase-locked pattern in the normalized $m = 0$ radial magnetic field at the reversal surface, $\hat{b}_r^{m=0}$, in our example RFP equilibrium, calculated as a function of the toroidal angle, ϕ, for various different values of β_0. This pattern is calculated from Eq. (203) on the assumption that $\hat{\Psi}^{0,n} \propto (\Delta^{0,n})^2$, which is consistent with an unstable $(0, n)$ tearing mode saturating at an amplitude such that the associated magnetic island width is proportional to $\Delta^{0,n}$ [see Eq. (175)]. For the sake of example, we have selected $\Delta_0 = +\pi/2$. It can be seen that $\hat{b}_r^{m=0}(\phi)$ exhibits a characteristic positive spike[19] at a particular toroidal angle, ϕ_0. (If $\Delta_0 = -\pi/2$ then the spike is negative.) As β_0 is gradually increased from a small value, the spike initially becomes more sharply defined, as more and more unstable $m = 0$ modes are incorporated into the phase-locked pattern. However, the spike dissipates somewhat as the beta limit is approached, because the (0, 1) mode amplitude becomes much larger than those of the other $m = 0$ modes.

D. Overlap integral

Figure 5 shows the incomplete overlap integral, $\int_0^{\hat{r}} \hat{\tau}(\hat{r}')\, d\hat{r}'$, and its integrand, calculated from the linear tearing eigenfunctions shown in Fig. 2. The island widths at the three rational surfaces are given the plausible values $\hat{W}^{1,8} = \hat{W}^{0,1} = \hat{W}^{1,9} = 0.01$. It can be seen that the equilibrium pressure gradient significantly increases the magnitude of, and changes the sign of, the complete overlap integral, $\int_0^1 \hat{\tau}(\hat{r})\, d\hat{r}$, relative to that in a zero pressure equilibrium. A significant increase in the magnitude of the complete overlap integral signifies a much stronger nonlinear coupling between the (1, 8), (0, 1), and (1, 9) tearing modes in a finite pressure equilibrium, compared to that in a zero pressure equilibrium, at fixed mode amplitude (see Sec. IV D). Moreover, the sign of overlap integral affects the relative phase relation between the phase-locked $m = 0$ and the $m = 1$ interference maxima (see Sec. VI E). Thus, we can appreciate that the incorporation of the equilibrium pressure profile into the analysis is of crucial importance when calculating the nonlinear coupling of tearing modes in an RFP.

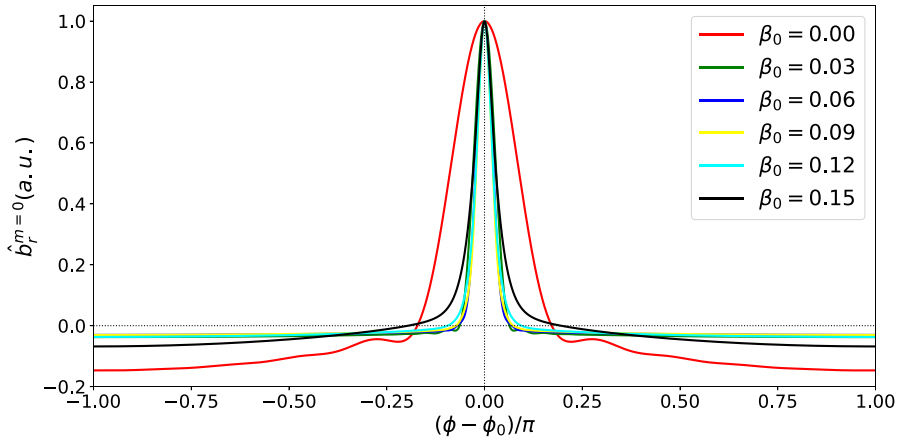

FIG. 4. Radial magnetic field of phase-locked $m = 0$ modes at the reversal surface in a stepped pressure RFP equilibrium characterized by $\epsilon_a = 0.25$, $q_0 = 0.14$, $\alpha_\sigma = 4$, $\nu_\sigma = 1.6$, $\alpha_p = 4$, $\nu_p = 2$, $\hat{b} = 1.01$, and various different values of β_0. There are 500 equally spaced control surfaces in the plasma. Here, ϕ is the toroidal angle. Note that $\Delta_0 = +\pi/2$.

23 April 2024 14:39:08

© Author(s) 2024

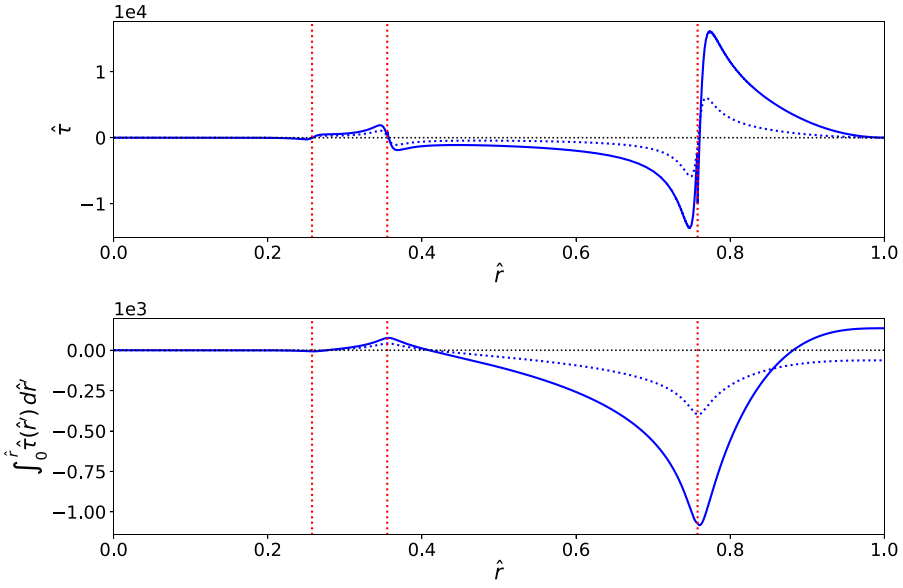

FIG. 5. The incomplete overlap integral, $\int_0^{\hat{r}} \hat{\tau}(\hat{r}')\, d\hat{r}'$, and its integrand, for the plasma equilibrium shown in Fig. 1 and the tearing eigenfunctions shown in Fig. 2. Here, $\hat{W}^{m_1,n_1} = \hat{W}^{m_2,n_2} = \hat{W}^{m_3,n_3} = 0.01$. The wall radius is $\hat{b} = 1.01$. There are 500 equally spaced control surfaces in the plasma. The vertical lines indicate the locations of the rational surfaces. The dotted curves show the zero pressure cases. Here, $\hat{r}$ represents normalized radial distance from the magnetic axis.

E. $m = 1$ modes

Figure 6 shows the tearing stability indices of the unstable $m = 1$ modes in our example RFP equilibrium, calculated as functions of the normalized equilibrium plasma pressure, β_0. There are no unstable $m = 1$ modes at zero pressure. However, it can be seen that there are 18 unstable tearing modes when $\beta_0 = 0.03$. Moreover, as the pressure is further increased, more and more modes become unstable. In all cases, the tearing stability index, $\Delta^{1,n}$, initially increases with increasing toroidal mode number, n, but eventually decreases.

Figure 7 shows the cosine and sine components (in the poloidal angle) of the phase-locked pattern in the normalized radial $m = 1$ magnetic field at the reversal surface, $C^{m=1}$ and $S^{m=1}$, respectively, in our example RFP equilibrium, calculated as functions of the toroidal angle, ϕ, for various different values of β_0. These patterns are calculated from Eqs. (214) and (215) on the assumption that $\hat{\Psi}^{1,n} \propto (\Delta^{1,n})^2$, which is consistent with an unstable $(1, n)$ tearing mode saturating at an amplitude such that the associated magnetic island width is proportional to $\Delta^{1,n}$. It can be seen that both $C^{m=1}(\phi)$ and $S^{m=1}(\phi)$ are strongly peaked at a particular toroidal angle, ϕ_1. As β_0 is gradually increased from a small value, the peaking becomes more sharply defined, as more and more unstable $m = 1$ modes are incorporated into the phase-locked pattern.

Figure 8 shows the locking potential for $m = 1$ modes in our example RFP equilibrium, calculated for various different values of β_0. This potential is calculated from Eq. (212) on the assumption that $\hat{\Psi}^{m,n} \propto (\Delta^{m,n})^2$, which is consistent with an unstable (m, n) tearing mode saturating at an amplitude such that the associated magnetic island width is proportional to $\Delta^{m,n}$. We have again selected $\Delta_0 = +\pi/2$. Note that the locking potential incorporates 153, 741, 990, 1540, and 2080 triplets of unstable $m = 1$ and $m = 0$ tearing modes at $\beta_0 = 0.03$, 0.06, 0.09, 0.12, and 0.15, respectively. Now, ϕ_1 and ϕ_0 are the toroidal angular locations of the interference maxima of the phase-locked $m = 1$ and $m = 0$ modes, respectively, see Figs. 4 and 7. Moreover, the argument of the locking potential, $\phi_1 - \phi_0$, takes

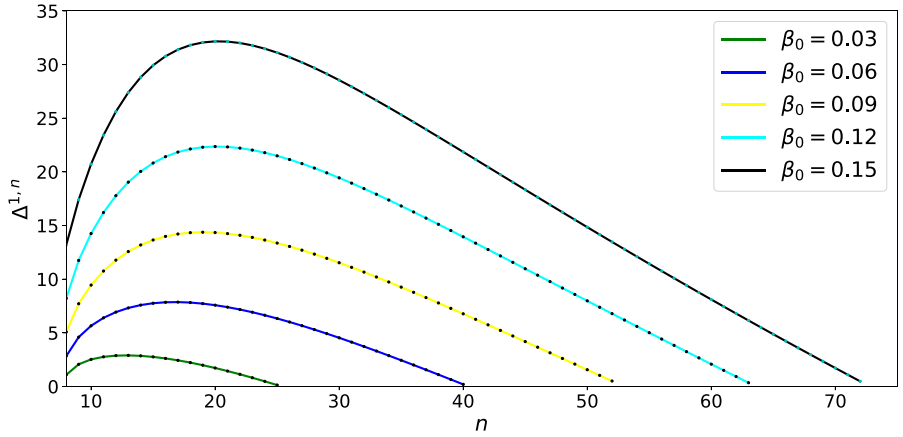

FIG. 6. Tearing stability indices of unstable $m = 1$ modes in a stepped pressure RFP equilibrium characterized by $\epsilon_a = 0.25$, $q_0 = 0.14$, $\alpha_\sigma = 4$, $\nu_\sigma = 1.6$, $\alpha_p = 4$, $\nu_p = 2$, $\hat{b} = 1.01$, and various different values of β_0. There are 500 equally spaced control surfaces in the plasma. Here, n is the toroidal mode number.

23 April 2024 14:39:08

© Author(s) 2024

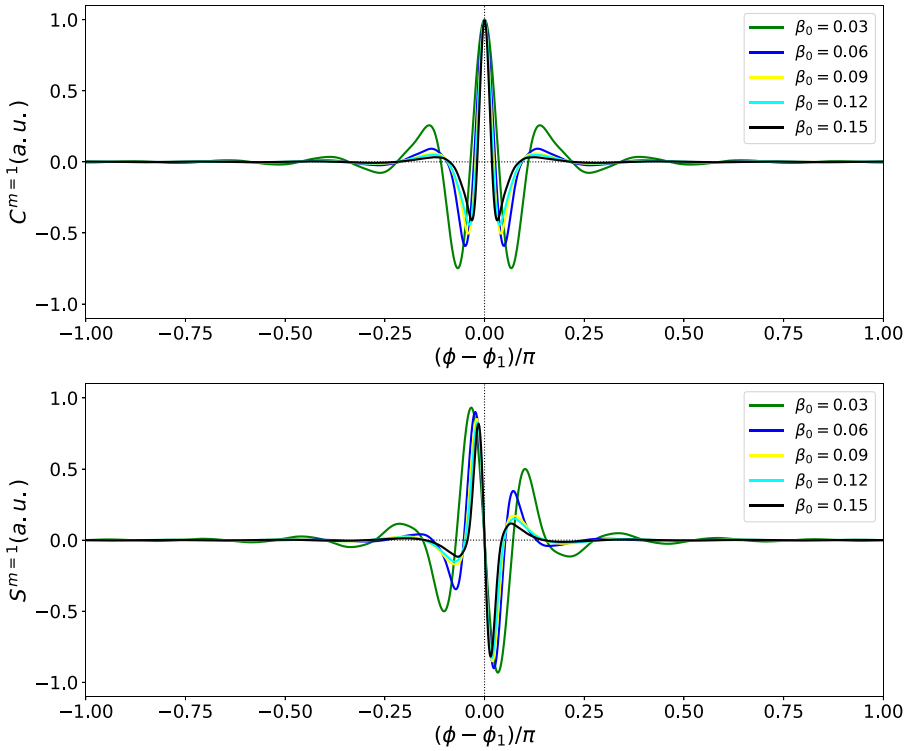

FIG. 7. Cosine and sine components (in the poloidal angle) of the radial magnetic field of phase-locked $m = 1$ modes at the reversal surface in a stepped pressure RFP equilibrium characterized by $\epsilon_a = 0.25$, $q_0 = 0.14$, $\alpha_\sigma = 4$, $\nu_\sigma = 1.6$, $\alpha_p = 4$, $\nu_p = 2$, $\hat{b} = 1.01$, and various different values of β_0. There are 500 equally spaced control surfaces in the plasma. Here, ϕ is the toroidal angle.

a value that minimizes the potential. It can be seen that $\phi_1 < \phi_0$ at comparatively low plasma pressures, whereas $\phi_1 > \phi_0$ at higher plasma pressures. This switch in sign of $\phi_1 - \phi_0$ is associated with a switch in sign of the overlap integrals (from negative at low pressures, to positive at high pressures). The magnitude of $|\phi_1 - \phi_0|$ decreases with increasing plasma pressure, implying a tighter coupling between the $m = 0$ and the $m = 1$ interference patterns, as more and more unstable triplets are incorporated into the slinky pattern. However, as the beta limit is approached, the (0, 1) mode starts to dominate, causing a dispersion of the $m = 0$ interference pattern (see Fig. 4), and an increase in $|\phi_1 - \phi_0|$. Note that the sign of $\phi_1 - \phi_0$ is swapped when $\Delta_0 = -\pi/2$.

The RFX experimental data discussed in Ref. 19 indicate that $\Delta_0 = +\pi/2$ [i.e., the spike in $b_r^{m=0}(\phi)$ is positive], which suggests, from the previous analysis, that $\phi_1 < \phi_0$ at low plasma pressures, and $\phi_1 > \phi_0$ at high plasma pressures. In fact, the observed value of $\phi_1 - \phi_0$ in RFX was negative, which is consistent with our low pressure results.

VII. SUMMARY

A theory of the three-wave coupling of triplets of tearing modes in toroidal pinches (i.e., either RFPs or tokamaks) was proposed in Ref. 18. However, this theory only applies to toroidal pinches with negligible equilibrium plasma pressure gradients. Such a limitation is

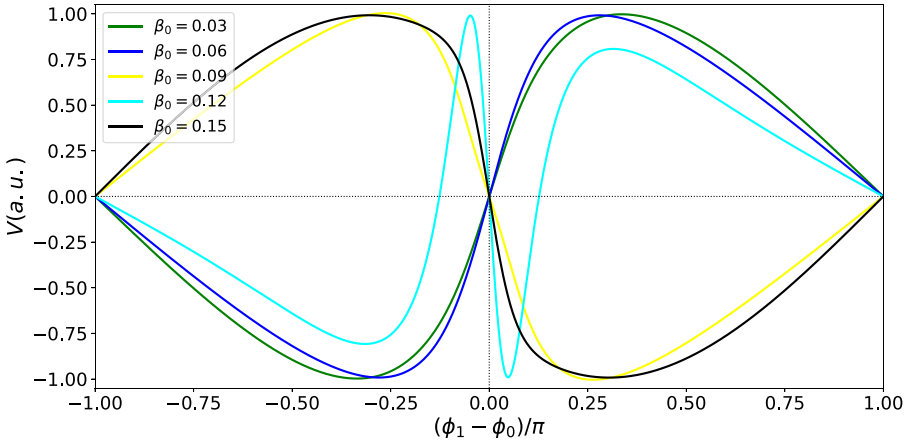

FIG. 8. Locking potential for $m = 1$ modes in a stepped pressure RFP equilibrium characterized by $\epsilon_a = 0.25$, $q_0 = 0.14$, $\alpha_\sigma = 4$, $\nu_\sigma = 1.6$, $\alpha_p = 4$, $\nu_p = 2$, $\hat{b} = 1.01$, and various different values of β_0. There are 500 equally spaced control surfaces in the plasma. Here, ϕ_0 and ϕ_1 are the toroidal angular locations of the interference maxima of the phase-locked $m = 0$ and $m = 1$ modes, respectively. $\phi_1 - \phi_0$ takes the value that minimizes the potential. Note that $\Delta_0 = +\pi/2$.

23 April 2024 14:39:08

© Author(s) 2024

particularly inappropriate to RFPs. In this paper, we generalize the analysis of Ref. 18 in order to take the equilibrium pressure gradient into account. However, for the sake of simplicity, we employ a stepped pressure profile, rather than a continuous profile. In the limit of a large number of pressure steps, it seems reasonable to expect the result of the stepped pressure calculation to be the same as that obtained from a continuous pressure calculation. However, the continuous pressure calculation has not been performed.

We have used our generalized theory of three-wave coupling to investigate the formation of the characteristic toroidally localized pattern of phase-locked $m = 1$ and $m = 0$ tearing modes in RFP plasmas that is known as the *slinky* pattern. We find that the incorporation of the equilibrium plasma pressure into the analysis is of crucial importance when determining the properties of this pattern. This is the case because the plasma pressure controls the number of unstable $m = 1$ and $m = 0$ tearing modes, and also significantly affects the strength of three-wave coupling, as well as the phase relation between the phase-locked $m = 1$ and $m = 0$ modes. Our predictions of the properties of the slinky pattern are, in general, agreement with experimental observations.[19]

In future work, we hope to apply our generalized theory to investigate the triggering of neoclassical tearing modes in tokamak plasmas via three-wave coupling.

ACKNOWLEDGMENTS

This research was directly funded by the U.S. Department of Energy, Office of Science, Office of Fusion Energy Sciences, under Contract No. DE-SC0021156.

AUTHOR DECLARATIONS

Conflict of Interest

The authors have no conflicts to disclose.

Author Contributions

R. Fitzpatrick: Conceptualization (lead); Formal analysis (lead); Funding acquisition (lead); Writing – original draft (lead).

DATA AVAILABILITY

The data that support the findings of this study are available from the corresponding author upon reasonable request.

REFERENCES

[1]J. A. Wesson and D. J. Campbell, *Tokamaks*, 4th ed. (Oxford University Press, Oxford, UK, 2011).
[2]H. A. B. Bodin, Nucl. Fusion **30**, 1717 (1990).
[3]L. Marrelli, P. Martin, M. E. Puiatti, J. S. Sarff, B. E. Chapman, J. R. Drake, D. F. Escande, and S. Masamune, Nucl. Fusion **61**, 023001 (2021).
[4]J. P. Freidberg, *Ideal Magnetohydrodynamics* (Plenum, New York, NY, 1987).
[5]J. A. Wesson, Nucl. Fusion **18**, 87 (1978).
[6]R. Fitzpatrick, *Tearing Mode Dynamics in Tokamak Plasmas* (Institute of Physics, Bristol, UK, 2023).
[7]J. B. Taylor, Rev. Mod. Phys. **58**, 741 (1986).
[8]K. Kusano and T. Sato, Nucl. Fusion **27**, 821 (1987).
[9]S. Ortolani and D. D. Schnack, *Magentohydrodynamics of Plasma Relaxation* (World Scientific, Singapore, 1993).
[10]S. Assadi, S. C. Prager, and K. L. Sidikman, Phys. Rev. Lett. **69**, 281 (1992).
[11]R. J. LaHaye, T. N. Carlstrom, R. R. Goforth, G. L. Jackson, M. J. Schaffer, T. Tamano, and P. L. Taylor, Phys. Fluids **27**, 2576 (1984).
[12]T. Tamano, W. D. Bard, C. Chu, Y. Kondoh, R. J. LaHaye, P. S. Lee, M. Saito, M. J. Schaffer, and P. L. Taylor, Phys. Rev. Lett. **59**, 1444 (1987).
[13]K. Hattori, Y. Hirano, T. Shimada, Y. Yagi, Y. Maejima, I. Hirota, and K. Ogawa, Phys. Fluids B **3**, 3111 (1991).
[14]D. Raju, O. Sauter, and J. B. Lister, Plasma Phys. Controlled Fusion **45**, 369 (2003).
[15]B. Tobias, M. Chen, I. G. J. Classen, C. W. Domier, R. Fitzpatrick, B. A. Grierson, N. C. Luhmann, Jr., C. M. Muscatello, M. Okabayashi, K. E. J. Olofsson, and C. Paz-Soldan, Phys. Plasmas **23**, 056107 (2016).
[16]L. Bardóczi, N. C. Logan, and E. J. Strait, Phys. Rev. Lett. **127**, 055002 (2021).
[17]M. F. F. Nave, E. Lazzaro, R. Coelho, P. Belo, D. Borba, R. J. Buttery, S. Nowak, F. Serra, and EFDA-JET Contributors, Nucl. Fusion **43**, 179 (2003).
[18]R. Fitzpatrick, Phys. Plasmas **6**, 1168 (1999).
[19]R. Fitzpatrick and P. Zanca, Phys. Plasmas **9**, 2707 (2002).
[20]R. Fitzpatrick, Phys. Plasmas **22**, 042514 (2015).
[21]M. J. Hole, S. R. Hudson, and R. L. Dewar, J. Plasma Phys. **72**, 1167 (2006).
[22]Z. S. Qu, R. L. Dewar, F. Ebrahimi, J. K. Anderson, S. R. Hudson, and M. J. Hole, Plasma Phys. Controlled Fusion **62**, 054002 (2020).
[23]C. C. Hegna, Phys. Plasmas **3**, 4646 (1996).
[24]R. M. Coelho, E. Lazzaro, M. F. F. Nave, and F. Serra, Phys. Plasmas **6**, 1194 (1999).
[25]J. L. Shohet, B. R. Barmish, H. K. Ebraheem, and A. C. Scott, Phys. Plasmas **11**, 3877 (2004).
[26]S. C. Guo and M. S. Chu, Phys. Plasmas **11**, 4050 (2004).
[27]H. P. Furth, J. Killeen, and M. N. Rosenbluth, Phys. Fluids **6**, 459 (1963).
[28]R. Fitzpatrick, R. J. Hastie, T. J. Martin, and C. M. Roach, Nucl. Fusion **33**, 1533 (1993).
[29]R. Fitzpatrick, Phys. Plasmas **24**, 072506 (2017).
[30]B. R. Suydam, in *Proceedings of the Second United Nations International Conference on the Peaceful Uses of Atomic Energy* (United Nations, Geneva, 1958), Vol. 31, p. 157.
[31]C. Mercier, Nucl. Fusion **1**, 47 (1960).
[32]A. H. Glasser, J. M. Greene, and J. L. Johnson, Phys. Fluids **19**, 567 (1976).
[33]R. Fitzpatrick, Phys. Plasmas **1**, 3308 (1994).
[34]P. H. Rutherford, Phys. Fluids **16**, 1903 (1973).
[35]R. A. White, D. A. Monticello, M. N. Rosenbluth, and B. V. Waddell, Phys. Fluids **20**, 800 (1977).
[36]A. Thyagaraja, Phys. Fluids **24**, 1716 (1981).
[37]D. F. Escande and M. Ottaviani, Phys. Lett. A **323**, 278 (2004).
[38]F. Militello and F. Porcelli, Phys. Plasmas **1**, L13 (2004).
[39]R. J. Hastie, F. Militello, and F. Porcelli, Phys. Rev. Lett. **95**, 065001 (2005).
[40]R. Fitzpatrick, Nucl. Fusion **33**, 1049 (1993).
[41]Y. Yagi, H. Koguchi, H. Sakakita, S. Sekine, P. R. Brunsell, and J.-A. Malmberg, Phys. Plasmas **8**, 1625 (2001).

23 April 2024 14:39:08

© Author(s) 2024